

A Hybrid Optimal Control Approach to Maximum Endurance of Aircraft

Emily Oelberg

A Thesis

in

The Department

of

Electrical and Computer Engineering

Presented in Partial Fulfillment of the Requirements

for the Degree of

Master of Applied Science (Electrical and Computer Engineering) at

Concordia University

Montréal, Québec, Canada

August 2018

© Emily Oelberg, 2018

**CONCORDIA UNIVERSITY
SCHOOL OF GRADUATE STUDIES**

This is to certify that the thesis prepared

By: Emily Kara Oelberg

Entitled: A Hybrid Optimal Control Approach to Maximum Endurance of Aircraft

and submitted in partial fulfillment of the requirements for the degree of

Master of Applied Science (Electrical and Computer Engineering)

complies with the regulations of this University and meets the accepted standards with respect to originality and quality.

Signed by the final examining committee:

_____	Chair
Dr. A. Mohammadi	
_____	External Examiner
Dr. J.Y. Yu (CIISE)	
_____	Internal Examiner
Dr. K. Skonieczny	
_____	Supervisor
Dr. L. Rodrigues	

Approved by: _____
Dr. W.E. Lynch, Chair
Department of Electrical and Computer Engineering

_____ 20 _____

_____ Dr. Amir Asif, Dean,
Faculty of Engineering and Computer Science

Abstract

A Hybrid Optimal Control Approach to Maximum Endurance of Aircraft

Emily Oelberg

Aircraft performance optimization is a field of increasing interest, especially with the prevalent use of flight management systems (FMS) on commercial aircraft, as well as the growing field of autonomous aircraft. This thesis addresses the maximum endurance performance mode. Maximizing the endurance of an aircraft has several applications in data collection, surveillance, and commercial flights. Each of these applications may be best suited for different aircraft such as fixed-wing or quad-rotor vehicles, with power plants being either fuel-burning or electric.

The objectives of this thesis are to solve the maximum endurance problem using an optimal control framework for fixed-wing aircraft while developing a unified model of energy-depletion which encompasses both fuel-burning and all-electric aircraft. The unified energy-depletion model allows the results to be applied to turbojet, turbofan, turboprop, and all-electric aircraft. The problem of maximum endurance in cruise will be solved for a three-phase model of flight including climb, cruise, and descent. This problem is solved using a hybrid optimal control framework using a unified energy-depletion model.

One of the advantages of using an optimal control framework is the possibility to develop analytical solutions. The results of this thesis include a general solution for maximizing the endurance of fixed-wing aircraft, as well as specific analytical solutions for each aircraft configuration wherever possible. Some benefits of analytical solutions are that they require the least amount of computation time and provide insight into the problem including sensitivities and physical dependencies. Simulations are provided to validate the results in the case of specific aircraft configurations (turbojet, turbofan, turboprop, and all-electric).

Acknowledgments

Firstly, I would like to thank my thesis advisor Dr. Luis Rodrigues for his invaluable advice, support, and guidance during the course of my research.

I would like to thank MITACS and TRU Simulation + Training for their financial support. TRU Simulation provided tremendous support in the use of their flight simulators to collect data that went into this thesis.

I would also like to thank my friends and family for their support. Thank you to my friends and labmates in the HYCONS lab for your support: Michael, Alex, Julia, Mailis, Bruno, Maxim, Amir, Reza, Boshra, Diego, Whong, and Inma. Thank you for the good times that we've had over the past two years.

Last but not least, I would like to extend a very special thanks to my partner Patrick for his never-ending support and encouragement.

Contents

List of Figures	viii
List of Tables	x
List of Symbols	xi
1 Introduction	1
1.1 Motivation	1
1.2 Literature Survey	3
1.3 Contributions	5
1.4 Thesis Structure	6
2 Theoretical Preliminaries	8
2.1 Aircraft Performance	8
2.1.1 Atmospheric Model	8
2.1.2 Mission Profile	9
2.1.3 Flight Envelope	10
2.1.4 Flight Dynamics	12
2.1.5 Fuel Consumption Model	12
2.1.6 Battery Model	13
2.1.7 Energy-Depletion Dynamics	14
2.2 Optimal Control	16
2.2.1 Optimal Control Problem	16

2.2.2	Necessary Conditions of Optimality	17
2.2.3	Linear Optimization Problems	18
2.3	Hybrid Optimal Control	18
2.3.1	Hybrid Optimal Control Problem	19
2.3.2	Necessary Conditions of Optimality	22
2.4	Motivating Example: Constant Airspeed versus State-Feedback Control	23
3	Maximum Endurance in Cruise	29
3.1	Assumptions and Models	29
3.2	Maximum Endurance OCP	31
3.3	Maximum Endurance Solution	32
3.4	Solved Examples	34
3.4.1	Turbojet	34
3.4.2	Turbofan	35
3.4.3	Turboprop	39
3.4.4	All-Electric	41
3.5	Aircraft Configurations	42
3.5.1	Aircraft Parameters	42
3.5.2	Turbojet	42
3.5.3	Turbofan	42
3.5.4	Turboprop	47
3.5.5	All-Electric	49
3.6	Summary	50
4	Maximum Cruise Endurance over Climb, Cruise, and Descent	52
4.1	Assumptions and Models	52
4.2	Maximum Endurance OCP	55
4.3	Maximum Endurance Solution	57
4.4	Solved Examples	67
4.4.1	Turbojet	67

4.4.2	Turbofan	68
4.4.3	Turboprop	69
4.4.4	All-Electric	70
4.5	Aircraft Configurations	71
4.5.1	Aircraft Parameters	71
4.5.2	Turbojet	71
4.5.3	Turbofan	73
4.5.4	Turboprop	75
4.5.5	All-Electric	78
4.6	Summary	80
5	Conclusions	82
5.1	Main Conclusions	83
5.2	Extensions	83
	Bibliography	85

List of Figures

Figure 1.1	Examples of Endurance Aircraft	2
Figure 2.1	ISA Model for Air Density	10
Figure 2.2	Typical Mission Profile	10
Figure 2.3	Hybrid Automaton	21
Figure 3.1	Comparison of Maximum Endurance Airspeed	43
Figure 3.2	Comparison of Maximum Endurance Airspeed	44
Figure 3.3	Error Analysis	44
Figure 3.4	Error Upper Bound at 10,000 ft	45
Figure 3.5	Error Upper Bound at 30,000 ft	45
Figure 3.6	Comparison of Different Engine Configurations at 10,000 ft	46
Figure 3.7	Comparison of Different Engine Configurations at 30,000 ft	46
Figure 3.8	Comparison of Boeing 737 FMS	47
Figure 3.9	Optimal Airspeed Profiles	48
Figure 3.10	Sensitivity of Endurance to Air Density	48
Figure 3.11	Maximum Endurance as a Function of Cruising Altitude	49
Figure 3.12	Sensitivity of Endurance to Air Density	49
Figure 3.13	Maximum Endurance as a Function of Cruising Altitude	50
Figure 4.1	Hybrid Automaton	54
Figure 4.2	Optimal Airspeed and Thrust Profiles	72
Figure 4.3	Weight and Altitude Trajectories	72
Figure 4.4	Altitude Profiles for Scaled Thrust Input	73

Figure 4.5	Effect of Reduced Thrust Profile on Endurance	73
Figure 4.6	Optimal Airspeed and Thrust Profiles	74
Figure 4.7	Weight and Altitude Trajectories	74
Figure 4.8	Altitude Profiles for Scaled Thrust Input	75
Figure 4.9	Optimal Airspeed and Thrust Profiles	76
Figure 4.10	Weight and Altitude Trajectories	76
Figure 4.11	Altitude Profiles for Scaled Thrust Input	77
Figure 4.12	Effect of Reduced Thrust Profile on Endurance	77
Figure 4.13	Optimal Airspeed and Thrust Profiles	78
Figure 4.14	Weight and Altitude Trajectories	78
Figure 4.15	Altitude Profiles for Scaled Thrust Input	79
Figure 4.16	Effect of Reduced Thrust Profile on Endurance	79

List of Tables

Table 3.1	Aircraft Dynamics Parameters	31
Table 3.2	Summary of Aircraft Parameters	43
Table 3.3	Maximum Endurance for Different Aircraft	50
Table 3.4	Optimal Airspeed Feasibility	51
Table 4.1	Aircraft Dynamics Parameters in Climb and Descent	55
Table 4.2	Optimal Airspeed Profiles for Different Aircraft	80
Table 4.3	Maximum Endurance for Different Aircraft	80

List of Symbols

Aircraft Parameters

α	Angle of attack, <i>rad</i>
γ	Flight path angle, <i>rad</i>
a	Fuel flow coefficient
b	Fuel flow coefficient
C_{D0}	Parasitic drag coefficient
C_{D2}	Induced drag coefficient
D	Drag, <i>N</i>
e	Heating value of fuel, <i>J/kg</i>
E	Energy, <i>J</i>
h	Altitude, <i>m</i>
i	Battery current, <i>A</i>
L	Lift, <i>N</i>
P	Power, <i>N – m/s</i>
Q	Battery charge, <i>C</i>
S	Wing area, <i>m²</i>
S_{FC}	Thrust specific fuel consumption (turbojet and turbofan), <i>(N/s)/N</i>
S_{FC}	Thrust specific fuel consumption (turboprop), <i>(N/s)/(N – m/s)</i>
T	Thrust, <i>N</i>
U	Battery voltage, <i>V</i>
v	Airspeed, <i>m/s</i>

- W Weight, N
 x Horizontal position, m
 ω Horizontal component of wind speed, m/s

Atmospheric Constants

- ρ Air density, kg/m^3
 Γ Temperature lapse rate, K/m
 c Speed of sound, m/s
 g Gravitational acceleration, m/s^2
 R Gas constant, $J/mol - K$
 M Molecular weight of dry air, kg/mol
 \mathcal{T} Temperature, K
 \mathcal{P} Pressure, Pa

Boundary Value Times

- t Time, s
 t_0 Initial time
 t_c Time at top of climb
 t_d Time at top of descent
 t_d Final time

Chapter 1

Introduction

1.1 Motivation

Aircraft performance optimization is a field of growing interest, especially given the increasing demand in air traffic where passenger demand is expected to double over the next 20 years [1]. The performance of an aircraft can be optimized with respect to a number of different factors depending on the application. Some popular aircraft performance optimization problems include: maximum range, economy mode (minimum direct operating cost), minimum time, and maximum endurance. The scope of this thesis is limited to the maximum endurance problem. Commercial aircraft typically fly in economy mode, which is a trade-off problem between the costs associated with fuel and time aloft. However, there are specific instances in which a pilot may be required to loiter for an indefinite amount of time, for example in cases of airport congestion. In fact, some airports are so congested that a short period of holding is expected as a means of maximizing runway usage [2]. In these situations, the aircraft should be flown to maximize their endurance.

Unmanned aerial vehicles are also gaining popularity in a number of areas which include applications that require long endurance capabilities. Some examples of current applications are: search and rescue [3], inspection of power lines [4], border patrol [5], crop surveillance [6], and weather monitoring [7]. Some examples of aircraft which would require endurance capabilities are shown in Figure 1.1. The Airbus E-Fan is an electric aircraft with limited endurance, however as electric aircraft gain popularity they could be applied to other long endurance applications. NASA's global



(a) Airbus E-Fan. Photo by wiltshirespotter, distributed under a CC BY-SA 2.0 license. URL: [https://commons.wikimedia.org/wiki/File:F-WILE_\(14682652304\).jpg](https://commons.wikimedia.org/wiki/File:F-WILE_(14682652304).jpg)



(b) NASA Global Hawk. Photo by NASA/Tony Landis. URL: https://en.wikipedia.org/wiki/File:NASA_Dryden_Global_Hawk.jpg



(c) Boeing Phantom Eye. Photo by NASA/Bob Ferguson. URL: https://www.nasa.gov/centers/dryden/multimedia/imagegallery/Phantom_Eye/MCF13-0015-315.html

Figure 1.1: Examples of Endurance Aircraft

Hawk is a long endurance weather surveillance aircraft and the Phantom Eye is a long endurance hydrogen-powered turboprop aircraft.

For the scope of this thesis, only fixed-wing aircraft will be considered. However, within the family of fixed-wing aircraft, there are several types of power-plants available. This thesis aims at developing a unified solution for fixed-wing aircraft which will model the power-plant energy-depletion dynamics such that they can be readily applied to different engine configurations including fuel-burning aircraft as well as all-electric aircraft. Fuel-burning aircraft are most commonly used. However, electric aircraft are increasingly gaining popularity. It is therefore useful to develop a framework which includes these aircraft as well. For examples of electric aircraft the reader is referred to the Airbus E-fan [8] and the battery-powered research aircraft being developed by NASA

[9]. Moreover, the unified framework allows easy comparison between the characteristics of each aircraft type, and can therefore be used in selection of the most appropriate aircraft for a given application.

1.2 Literature Survey

Optimal control theory has been developed starting in the 1950's as an extension of calculus of variations [10, 11, 12, 13, 14]. In particular, optimal control has been used in aircraft performance optimization problems for over 50 years [15, 16]. This thesis aims at applying these techniques to solve the maximum endurance problem of fixed-wing aircraft in level-cruise with a model that includes head and tailwinds. Another objective of this thesis is to solve the problem for maximum cruise endurance over the climb, cruise, and descent phases of flight using a hybrid optimal control (HOC) framework. A comprehensive overview of the HOC framework is provided in [17] and [10] and the references therein.

Optimal control theory has been applied to various aircraft performance optimization problems. Often these are used for flight management system (FMS) algorithms. The FMS is an onboard computer used in commercial aircraft to perform a range of tasks such as: flight planning, navigation, and performance optimization. Several papers have been published dealing with the optimization of FMS algorithms, including the economy mode problem for jet aircraft in cruise [18, 19, 20, 21, 22]. A comparison of minimum-fuel optimization techniques for jet aircraft was provided in [23] for level-cruise flight with fixed arrival time. However, only numerical techniques were included in the comparison. The minimum fuel problem was solved for hybrid electric vehicles in [24] using Pontryagin's Maximum Principle, however only numerical results were provided. An optimal control framework was proposed for maximum endurance of jet aircraft in [15], and an expression for endurance of a turbofan was formulated in [25]. However, in both cases no optimal solution was provided. In [26], the approximate endurance time was derived from the maximum range solution for jet aircraft, but the proposed method assumes constant speed and is only proposed as a rough estimate. The maximum endurance problem was formulated and solved for a turbojet using an optimal control framework in [27] for the cruise portion of flight and the authors provided an analytical

state-feedback solution. Similarly, an analytical state-feedback solution to the maximum endurance problem for all-electric aircraft was proposed in [28, 29]. The maximum endurance problem of a turboprop in cruise was formulated and solved in [30] assuming constant airspeed. An expression for endurance of a turboprop in cruise was formulated in [25], but no optimal solution was given, and wind was not considered.

Although many references addressed the maximum endurance problem for various aircraft, to the best of the author's knowledge, the problem of maximum endurance has not been formulated using a unified energy-depletion model for fixed-wing aircraft with the inclusion of head and tailwinds in the model. In particular, no analytical state-feedback solution has been developed for the turbofan and turboprop aircraft in cruise.

Hybrid optimal control has been applied in several applications. For example, a hybrid optimal control framework was used in the control of an electric vehicle in [31] and a hybrid optimal control framework was proposed for launch vehicle mission planning in [32]. In [33], a hybrid optimal control framework was used to formulate the climb, cruise and descent phases of flight. However, the hybrid optimal control problem was then re-formulated as a classical optimal control problem and no analytical solution was given. A fixed-range minimum fuel problem for jet aircraft was formulated using a hybrid optimal control framework in [34] including climb, cruise, and descent. Numerical results were also provided. The different phases of flight are modelled using a hybrid system in [35]. However, to the best of the author's knowledge, a hybrid optimal control framework has not been applied to the maximum endurance problem in cruise.

Periodic cruise trajectories were developed in [36, 37] in order to maximize endurance in cruise. However, in these papers, the aircraft model assumes that the weight is constant and that the engine power can be set to zero. Furthermore, the proposed periodic trajectory requires the aircraft to be constantly climbing or descending between some maximum and minimum altitude, which is not practical for commercial flights as aircraft are required to maintain a given flight level determined by air traffic control. The climb and descent portions of flight were studied for the economy mode problem of a turbojet in [38]. The minimum fuel problem for descent of a jet aircraft with fixed arrival time was presented in [39]. Top of descent location was estimated for idle-thrust descent

trajectories in [40]. Furthermore, hybrid optimal control has been used in aircraft trajectory optimization. A unified approach was used to solve the maximum endurance and maximum range problem for propeller and jet aircraft in cruise in [41]. In [42], the specific energy is used as an independent variable to minimize the direct operating cost of an aircraft with fixed range over climb, cruise, and descent. Genetic algorithms were applied to optimize 3D flight profiles of aircraft with a model including wind in [43]. The advantage of this methodology is that the wind model that is used in the simulations can be more complex. However, no analytical solutions are provided.

To the best of the author's knowledge, the problem of maximum endurance for fixed-wing aircraft has not been solved using a hybrid optimal control approach using a unified energy-depletion model. Several papers have provided numerical solutions, however the advantage of the framework proposed in this thesis is that in many cases it provides analytical solutions.

In [44], the wind effect was incorporated as a final penalty in the economy mode problem. In [45], measured flight data was used to develop a modified Bréguet equation to incorporate the effect of wind on maximum range in cruise. The minimum fuel problem for jet aircraft was formulated with constant head and tailwinds in cruise and climb/descent separately in [46]. However, only numerical solutions were provided. The effect of horizontal head or tail-wind on maximum endurance and maximum range of a turbojet was already established in [47] and is in agreement with the theoretical results of this thesis. However, no formal proof was provided in [47].

1.3 Contributions

The main contributions of this thesis are as follows:

- The first contribution of this thesis is a unification of different aircraft power plant configuration models into a single energy-depletion model. This model captures the essential characteristic of the system, which is how energy is consumed, whether that energy be from fuel or battery charge.
- Next, in conjunction with the unified energy-depletion model, a hybrid optimal control framework was applied to solve the cruise maximum endurance problem over climb, cruise, and

descent. Since the energy-depletion model is used, the resulting solution is general for a family of fixed-wing aircraft power plant configurations.

- Then, from the above-mentioned framework, a series of analytical solutions are provided, including: an analytical solution for the maximum endurance problem of a turboprop in cruise, the sensitivity of the endurance to cruising altitude for the turboprop and all-electric aircraft, and analytical solutions for the climb, cruise, and descent phases of flight for the turbojet, turboprop, and all-electric aircraft.
- Finally, an approximate analytical solution for the maximum endurance problem of a turbofan is provided and then validated using a flight simulator Boeing 737 FMS.

1.4 Thesis Structure

Chapter 2 provides an overview of the aircraft performance and atmospheric models used later in the problem formulation. It also provides a general overview of the theory used in the problem solution, namely classical and hybrid optimal control theory. In addition, it provides a motivating example demonstrating the advantage of a state-feedback solution over a constant airspeed solution. Chapter 3 presents the problem of maximum endurance for an aircraft in cruise as well as a general solution of this problem. This general solution is then applied to specific cases of aircraft configurations, which are: turbojet, turbofan, turboprop, and all-electric. Simulation results are provided for each of these specific examples. Next, Chapter 4 follows the same format as Chapter 3, but formulates the problem to include the climb and descent portions of flight. Similarly, the general solution is given, followed by specific examples for different aircraft. Simulation results are also provided. Finally, Chapter 5 draws conclusions and suggests possible extensions for future work.

Some of the work of Chapter 3 has been published in

E. Oelberg, L. Rodrigues, "Maximum Endurance of a Turbofan in Cruise with Constant Head or Tail-Wind", *American Control Conference*, June 2018, Milwaukee, Wisconsin.

E. Oelberg, L. Rodrigues, "Maximum Endurance of a Turboprop in Cruise with Head and

Tail-Wind”, *31st Annual IEEE Canadian Conference on Electrical and Computer Engineering*, May 2018, Quebec City, Quebec.

Chapter 2

Theoretical Preliminaries

This chapter is broken down into two sections. The first section will provide the mathematical models, assumptions, and constraints which will represent the system. The second section will outline the mathematical techniques used to solve the maximum endurance problem.

2.1 Aircraft Performance

Before the problem of maximum endurance can be formulated, the system must be modelled mathematically. The scope of this thesis includes four types of aircraft: turbojet, turbofan, turbo-prop, and all-electric. Each of these aircraft has its own unique properties, and some properties are common across each. This section will illustrate the aspects of flight which must be modelled in order to accurately represent each of these aircraft while aiming at reaching a model which is as general as possible.

2.1.1 Atmospheric Model

The dynamics of the system depend on the density of air as a function of altitude. Therefore, an expression for $\rho(h)$ will be derived using the International Standard Atmosphere (ISA) model [48]. This model is valid for the troposphere. The equations from the ISA model are

$$\begin{aligned}
\mathcal{T}(h) &= \mathcal{T}_0 - \Gamma h \\
\mathcal{P}(h) &= \mathcal{P}_0 \left(1 - \frac{\Gamma h}{\mathcal{T}_0}\right)^{\frac{gM}{R\Gamma}} \\
\rho(h) &= \frac{M\mathcal{P}(h)}{R\mathcal{T}(h)}
\end{aligned} \tag{1}$$

where the constants in (1) have the following values

g = gravitational acceleration (9.81 m/s^2)

Γ = temperature lapse rate (0.0065 K/m)

R = gas constant (8.314 $J/molK$)

M = molecular weight of dry air (0.02896 kg/mol)

\mathcal{T}_0 = standard sea level temperature (288.15 K)

\mathcal{P}_0 = standard sea level pressure (101,325 Pa)

Solving for $\rho(h)$ yields

$$\rho(h) = \frac{M\mathcal{P}_0}{R\mathcal{T}_0} \left(1 - \frac{\Gamma h}{\mathcal{T}_0}\right)^{\frac{gM}{R\Gamma} - 1} \tag{2}$$

and is shown in Figure 2.1. The first derivative of ρ with respect to altitude is

$$\rho_h = \frac{M\mathcal{P}_0(R\Gamma - gM)}{R^2\mathcal{T}_0^2} \left(1 - \frac{\Gamma h}{\mathcal{T}_0}\right)^{\frac{gM}{R\Gamma} - 2} < 0 \tag{3}$$

which is strictly negative since air density decreases with altitude.

2.1.2 Mission Profile

The mission profile of the aircraft will be treated as consisting of three separate phases: climb, cruise, and descent. A typical mission profile for a commercial aircraft is shown in Figure 2.2 where

t_0 = Initial time

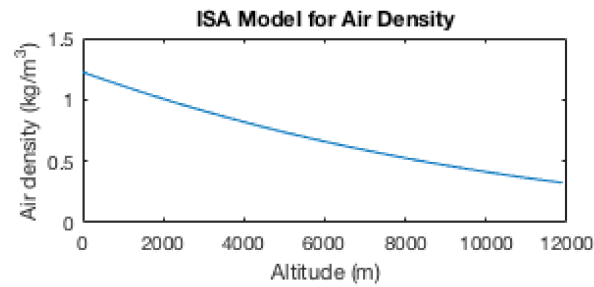


Figure 2.1: ISA Model for Air Density

t_c = Time at top of climb

t_d = Time at top of descent

t_f = Final time

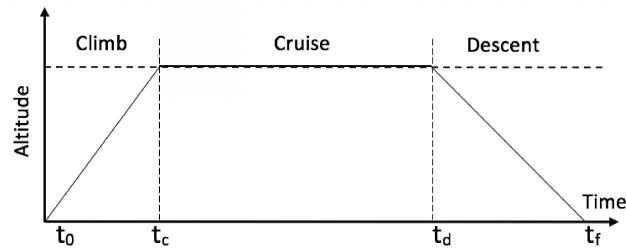


Figure 2.2: Typical Mission Profile

2.1.3 Flight Envelope

To ensure flight safety, we must verify that the solutions obtained produce controls that fall within the flight envelope of the aircraft. Each aircraft was designed to operate within a given range of parameters. The constraints relevant to the scope of this thesis are presented below and can be found in [49, 50, 51].

Stall Speed

In order to maintain a level flight, an aircraft must fly above its stall speed. The stall speed of an aircraft will depend on a number of factors, namely the altitude, weight, and maximum lift coefficient of the aircraft

$$v_{stall} = \sqrt{\frac{2W}{\rho S (C_L)_{max}}} \quad (4)$$

Maximum Operating Mach Number

The aircraft must fly below its maximum operating Mach number, otherwise it may experience stability or structural problems. The maximum operating Mach number is aircraft specific.

Service Ceiling

The altitude at which the available rate of climb of an aircraft is zero represents the absolute ceiling of an aircraft, since it cannot climb further. The service ceiling is a lower altitude defined by the altitude at which the maximum rate of climb of the aircraft is 100 ft/min. It will be assumed in this thesis that all aircraft fly below their service ceiling.

Thrust Constraints

Aircraft are limited by the maximum and minimum thrust that their power-plant can produce. In climb, there will be some maximum thrust available to the aircraft which will depend on altitude and the aircraft parameters.

For turboprops, the maximum power available depends on altitude and is given by

$$P_{max}(h) = P_s \left(\frac{\rho(h)}{\rho_s} \right)^n \quad (5)$$

where P_s is the maximum available power at sea level, ρ_s is the air density at sea level, and $n = 0.7$ for turboprops [49]. The maximum thrust at positive speed v is given by

$$T_{max}(v, \rho) = \frac{P_{max}(h)}{v} \quad (6)$$

For turbojet and turbofan aircraft, the available thrust does not depend on airspeed, only on altitude. The relationship between maximum thrust and altitude is

$$T_{max}(h) = T_s \left(\frac{\rho(h)}{\rho_s} \right)^m \quad (7)$$

where T_s is the available thrust at sea level, ρ_s is the air density at sea level, and m is an engine specific constant coefficient.

In descent, the minimum thrust an engine can produce is idle thrust. The idle thrust is assumed to be constant and aircraft dependent.

2.1.4 Flight Dynamics

The following dynamics are common for all aircraft described in this thesis. The groundspeed is given by

$$\dot{x} = v \cos \gamma + \omega \quad (8)$$

where ω represents the horizontal component of wind, and v is the airspeed and γ is the flight path angle. Neglecting the vertical windspeed component, the rate of climb/descent is given by

$$\dot{h} = v \sin \gamma \quad (9)$$

where γ is positive for climb, negative for descent, and zero for level cruise.

For positive v , the dynamics in v and γ are

$$\dot{v} = \frac{g}{W} (T \cos \alpha - D - W \sin \gamma) \quad (10)$$

$$\dot{\gamma} = \frac{g}{vW} (T \sin \alpha + L - W \cos \gamma) \quad (11)$$

The drag on the aircraft will be given by the drag polar

$$D = \frac{1}{2} \rho S C_{D0} v^2 + \frac{2C_{D2} W^2}{\rho S v^2} \quad (12)$$

2.1.5 Fuel Consumption Model

For fuel-powered aircraft, the aircraft weight will decrease during flight as fuel is burned. These weight dynamics depend on the specific fuel consumption, S_{FC} . For turbojet and turbofan aircraft,

specific fuel consumption represents the ratio of fuel-flow rate (N/s) over thrust (N). For turboprop aircraft, specific fuel consumption represents the ratio of fuel-flow rate (N/s) over power (N-m/s).

The specific fuel consumption for turbofan and turbojet aircraft is given by [50]

$$S_{FC} = \left(a + b \frac{v}{c} \right) \delta(h) \quad (13)$$

where

$$\delta(h) = \sqrt{1 - \frac{\Gamma h}{\mathcal{T}_0}} \quad (14)$$

where Γ is the temperature lapse rate and \mathcal{T}_0 is the standard sea level temperature, a and b are constant fuel flow coefficients, and c is the speed of sound in air. However, the effect of $\delta(h)$ is relatively small and will be neglected. For turboprop aircraft, specific fuel consumption is assumed to be independent of airspeed and altitude [49].

The weight dynamics of fuel-burning aircraft will be modelled as

$$\dot{W} = -S_{FC}T \quad (15)$$

for turbojet and turbofan aircraft, and

$$\dot{W} = -S_{FC}Tv \quad (16)$$

for turboprop aircraft.

All-electric aircraft do not burn fuel for energy and instead deplete charge of a battery. The battery dynamics will be discussed in the following section.

2.1.6 Battery Model

Electric aircraft are powered by stored energy in the form of battery charge. Instead of burning fuel, the charge of the battery is depleted.

The following assumptions will be made regarding the battery, and are taken from [28]

Assumption 2.1.1. *The internal resistance of the battery will be neglected*

Assumption 2.1.2. *The battery's output voltage is assumed to be constant*

Assumption 2.1.3. *The electromotive force does not depend on the temperature of the battery*

Assumption 2.1.4. *The battery capacity does not depend on the amplitude of the current*

Using Assumptions 2.1.1 to 2.1.4, the charge dynamics of the battery will be derived. The required power for an all-electric aircraft is

$$P = Tv \tag{17}$$

The charge dynamics of an ideal battery are

$$\dot{Q} = i \tag{18}$$

According to Ohm's law, the current is

$$i = \frac{P}{U} \tag{19}$$

Substituting (17) into (19), and then (19) into (18) yields

$$\dot{Q} = \frac{Tv}{U} \tag{20}$$

2.1.7 Energy-Depletion Dynamics

Four types of aircraft will be modelled in this thesis. The main difference between these aircraft is the way in which they generate power. Turbojet, turbofan, and turboprop aircraft all burn fuel to generate energy, and therefore their weight decreases during flight as fuel is consumed. On the other hand, all-electric aircraft maintain a constant weight during flight and the energy expended comes from stored battery charge. In order to model the dynamics of these four aircraft using the same framework, the weight and charge dynamics will be converted into energy dynamics.

This section will derive the conversion from fuel and charge to energy, respectively, so that the maximum endurance optimal control problem can be formulated more generally.

Fuel to Energy

Aviation fuel is a class of fuel used to power aircraft engines. One important property of fuel is its heating value. The heating value of fuel is constant, and represents the energy stored per kilogram of fuel. Typical values for jet fuel range from 40,000 kJ/kg to 43,000 kJ/kg [50]. The weight dynamics of the fuel-powered aircraft can therefore be converted to energy dynamics by multiplying the weight dynamics by the heating value, e , of the fuel used. The time rate of change of energy for a fuel powered aircraft is

$$\dot{E} = e\dot{W} \quad (21)$$

Similarly, the weight boundary conditions can be converted to energy boundary conditions using the following relationship

$$E = eW_{fuel} \quad (22)$$

Charge to Energy

The energy stored in a battery is given by

$$E = QU \quad (23)$$

Using Assumption 2.1.2, the first time derivative of energy is

$$\dot{E} = \dot{Q}U \quad (24)$$

Replacing (20) into (24) yields the charge dynamics for an all-electric aircraft

$$\dot{E} = Tv \quad (25)$$

which has units of time rate of change of energy (J/s).

Furthermore, the boundary conditions of the system can be converted from charge to energy

using the relationship (23).

2.2 Optimal Control

Optimal control theory has been developed starting in the 1950's as an extension of calculus of variations [10, 11, 12, 13, 14]. In this thesis, subscript notation will be used for partial derivatives. That is, the partial derivative of H with respect to x will be written as H_x .

2.2.1 Optimal Control Problem

An optimal control problem (OCP) includes: a performance index (or cost functional), state dynamics, terminal cost functions, boundary conditions, and control inputs. The performance index will be defined as

$$J = \int_{t_0}^{t_f} L(x(t), u(t), t) dt \quad (26)$$

where x represents the set of state variables, u is the set of control inputs, t_0 and t_f are initial and final times, and L is a cost function. The system will be modelled using state dynamics defined as

$$\dot{x} = f(x(t), u(t), t) \quad (27)$$

where the initial conditions of the states are assumed to be known, and the end point conditions of the states may be fixed or free. The states may be specified at final time by a terminal constraint equation

$$\psi(x(t_f), t_f) = 0 \quad (28)$$

The optimal control problem can therefore be written as

$$\begin{aligned}
J^* &= \max \left\{ \int_{t_0}^{t_a} L(x(t), u(t), t) dt \right\} \\
&\text{s.t.} \\
\dot{x} &= f(x(t), u(t), t) \\
x(t_0) &= x_0 \\
\psi(x(t_f), t_f) &= 0
\end{aligned} \tag{29}$$

2.2.2 Necessary Conditions of Optimality

Define the Hamiltonian as

$$H(x(t), u(t), J_x, t) = J_x^{*T} f(x(t), u(t), t) + L(x(t), u(t), t) \tag{30}$$

where J_x is called the adjoint vector or costate, f is the system dynamics, and L is the cost function. The following theorem gives the necessary conditions of optimality, and is adapted from [10, 12].

Theorem 1. *If u^* is an optimal control input trajectory for problem (29) and x^* is the corresponding optimal state trajectory, then there exists a costate J_x^* such that*

$$\dot{J}_x^* = -\frac{\partial H}{\partial x}, \quad \dot{x} = \frac{\partial H}{\partial J_x^*} \tag{31}$$

where the boundary conditions on the states and costates are

$$x^*(t_0) = x_0, \quad J_x^*(t_f) = \nu^T \frac{\partial \psi(x(t_f), t_f)}{\partial x(t_f)} \tag{32}$$

where ν^T is a constant vector. Furthermore, the necessary condition of optimality is

$$\frac{\partial H}{\partial u} = 0 \tag{33}$$

A proof of Theorem 1 can be found in [10].

2.2.3 Linear Optimization Problems

A special case of (29) occurs when both the performance index and the constraints are linear in one or more of the control variables. This is referred to as a linear optimization problem (LOP). In this case, the necessary condition (33) in Theorem 1 cannot be used to determine the control input that only appears linearly. The following theorem is adapted from [12] and gives the necessary condition for a maximum in the case of a LOP.

Theorem 2. *For a control input u which only appears linearly in the performance index and constraints of problem (29), define the switching function ζ as*

$$\frac{\partial H}{\partial u} = \zeta \quad (34)$$

and let u be bounded by

$$u_{min} \leq u \leq u_{max} \quad (35)$$

then the optimal control input u^* which maximizes the cost functional is

$$u^* = \begin{cases} u_{max} & \text{if } \zeta > 0 \\ u_{min} & \text{if } \zeta < 0 \\ u_{sing} & \text{if } \zeta = 0 \end{cases} \quad (36)$$

where u_{sing} is called a singular solution, and is found by differentiating ζ with respect to time repeatedly until the control u appears explicitly.

The proof of Theorem 2 is available in [12]. Further details and a proof of the necessary conditions for singular solutions are available in [52, 53, 54, 55].

2.3 Hybrid Optimal Control

The classical optimal control framework can be readily applied to solve flight performance optimization problems in cruise, including the maximum endurance, maximum range, minimum

time, and economy mode problems. These problems can be solved using the framework described in Section 2.2. However, this thesis will also address the problem of maximum endurance with a model that includes the climb, cruise, and descent phases of flight. Including the three phases of flight introduces two main complications to the optimal control problem:

- The system will have a different set of state space dynamics for each phase of flight (climb, cruise, and descent)
- Due to the nature of a typical mission profile, the system will have interior boundary constraints at the switching instances (for example, a target cruising altitude, and a minimum required weight or battery charge required before descent)

In order to capture these additional complexities, a hybrid optimal control framework will be used. Hybrid optimal control is an extension of the classical optimal control theory reviewed in Section 2.2 which allows for discrete switches to occur in the system. In particular, the properties of a hybrid optimal control problem relevant to this thesis are

- Interior point constraints on the states at switching instants
- Changes in the state-space dynamics and of the state-space dimension at switching instants

These differences will be explained in more detail in the following section.

2.3.1 Hybrid Optimal Control Problem

A hybrid optimal control framework is provided in [17] and [10]. We will begin by defining the notation that will be used. The superscript (i) will represent the dynamics or constraints for a given discrete state i . The subscript i will be used to indicate the time of switching from state $i - 1$ to i . The notation t_{i-} refers to the time just before t_i , and t_{i+} refers to the time immediately after.

Thus, for N discrete system states, the dynamics at each state will be defined as

$$\dot{x} = f^{(i)}(x(t), u(t), t), \quad t_i < t < t_{i+1}, \quad i = 0, \dots, N - 1 \quad (37)$$

and at each switching instant t_i , $i = 1, \dots, N - 1$ the dimension of the state space may change. Furthermore, each switching instant t_i will be defined by a switching manifold as

$$\psi^{(i)}(x(t_i), t_i) = 0 \quad (38)$$

In other words, (38) indicates the time t_i at which the system's discrete state switches from discrete state $i - 1$ to discrete state i . The switching manifold (38) is similar to the function of the terminal state ψ in Section 2.2.1, except that for a hybrid system, there can be a function of the state $\psi^{(i)}$ at each switching instant t_i . These functions are used to specify the state at the switching times and the final time.

The performance index is defined similarly to (26) in Section 2.2.1. However, there will be a cost function $L^{(i)}$ for each state. The hybrid system cost functional is

$$J = \sum_{i=0}^{N-1} \left(\int_{t_i}^{t_{i+1}} L^{(i)}(x(t), u(t), t) dt \right) \quad (39)$$

However, in the case of maximum endurance in cruise, only the cruise endurance time will be maximized. Therefore, the cost functional will be

$$J = \int_{t_1}^{t_2} dt \quad (40)$$

where t_1 is the time at top of climb and t_2 is the time at top of descent.

From (37), (38), and (39), the hybrid optimal control problem can be formulated as

$$\begin{aligned} J^* = \max & \left\{ \sum_{i=0}^{N-1} \left(\int_{t_i}^{t_{i+1}} L^{(i)}(x(t), u(t), t) dt \right) \right\} \\ & s.t. \\ & \dot{x} = f^{(i)}(x(t), u(t), t), \quad t_i < t < t_{i+1}, \quad i = 0, \dots, N - 1 \\ & x(t_0) = x_0 \\ & \psi^{(i)}(x(t_i), t_i) = 0, \quad i = 1, \dots, N \end{aligned} \quad (41)$$

For the scope of this thesis, the system to be modelled is the flight dynamics of an aircraft over

its mission profile. The system states will be climb, cruise, and descent. The system will experience two switches: 1) climb to cruise and 2) cruise to descent. At each switch the dimension of the state space will change and the state dynamics will change. The relevant switching times are defined as

t_0 Initial time

t_1 Top of climb, switch from climb to cruise (corresponds to t_c in Figure 2.2)

t_2 Top of descent, switch from cruise to descent (corresponds to t_d in Figure 2.2)

t_3 Final time (corresponds to t_f in Figure 2.2)

The first switch from climb to cruise will be defined by the switching manifold

$$\psi^{(1)} = h(t_1) - h_c = 0 \quad (42)$$

where h_c is the desired cruising altitude. The second switch from cruise to descent will be defined by the switching manifold

$$\psi^{(2)} = E(t_2) - E_d = 0 \quad (43)$$

where E_d is the minimum energy the aircraft requires for safe descent.

A hybrid automaton of the switched system for the three phases of the mission profile of an aircraft is given in Figure 2.3 where q represents the discrete state of flight, f is the state variable dynamics, $\psi^{(1)}$ and $\psi^{(2)}$ are switching manifolds.

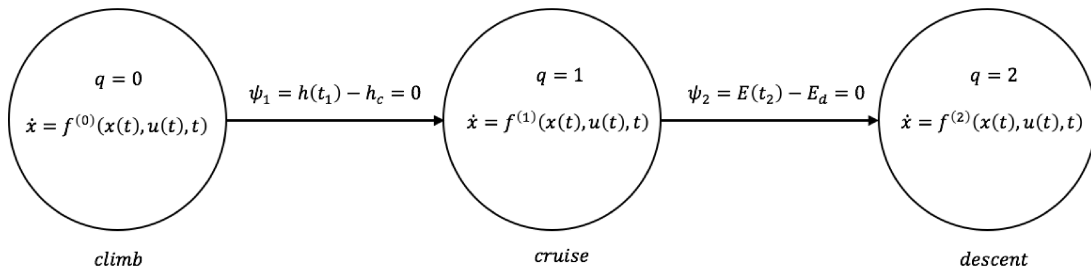


Figure 2.3: Hybrid Automaton

2.3.2 Necessary Conditions of Optimality

The hybrid optimal control framework is described in [10, 17]. First, for N discrete states, define a family of Hamiltonians as

$$H^{(i)}(x(t), u(t), J_x(t), t) = J_x^{*T} f^{(i)}(x(t), u(t), t) + L^{(i)}(x(t), u(t), t), \quad i = 0, \dots, N-1 \quad (44)$$

where J_x^* is a costate vector. This formulation is similar to (30) in Section 2.2.1. However, in the case of a switched system, the costate vector and Hamiltonian are not necessarily continuous and may experience jump discontinuities at the switching instants. The following theorem provides the necessary conditions of optimality and is adapted from [10, 17].

Theorem 3. *At switching instants t_i , $i = 1, \dots, N - 1$, the Hamiltonian may experience a jump discontinuity according to*

$$H^{(i-1)}(t_{i-}) = H^{(i)}(t_{i+}) - \nu^{(i)T} \left(\frac{\partial \psi^{(i)}(x(t_i), t_i)}{\partial t_i} \right) \quad (45)$$

where $\nu^{(i)}$ is a constant vector.

For each discrete state $^{(i)}$ where $u^{*(i)}$ is an optimal control input trajectory and $\dot{x} = f^{(i)}$ is the corresponding state trajectory, there exists a costate J_x^* such that

$$\dot{J}_x^* = -\frac{\partial H^{(i)}}{\partial x}, \quad f^{(i)} = \frac{\partial H^{(i)}}{\partial J_x^*}, \quad t_i < t < t_{i+1}, \quad i = 0, \dots, N-1 \quad (46)$$

and J_x^* is not necessarily continuous at the switching instants t_i , $i = 1, \dots, N - 1$. The interior boundary conditions on J_x^* are

$$J_x^*(t_{i-}) = J_x^*(t_{i+}) + \nu^{(i)T} \left(\frac{\partial \psi^{(i)}(x(t_i), t_i)}{\partial x(t_i)} \right), \quad i = 0, \dots, N-1 \quad (47)$$

Finally, the necessary condition in the control input u is given at each discrete state by

$$\frac{\partial H^{(i)}}{\partial u} = 0, \quad t_i < t < t_{i+1}, \quad i = 1, \dots, N-1 \quad (48)$$

The proof of Theorem 3 is available in [17].

2.4 Motivating Example: Constant Airspeed versus State-Feedback Control

The maximum endurance problem of a turbojet in cruise was already solved using an optimal control framework in [27]. The maximum endurance airspeed of a turbojet is

$$v^* = \sqrt{\frac{2W}{\rho S} \sqrt{\frac{C_{D2}}{C_{D0}}}} \quad (49)$$

which is a state-feedback controller which depends on weight W and several constants (for a constant altitude). The total endurance time is the well-known Breguet equation

$$J^* = \frac{1}{2S_{FC}\sqrt{C_{D0}C_{D2}}} \ln\left(\frac{W_c}{W_d}\right) \quad (50)$$

where W_c is the weight at top of climb and W_d is the weight at top of descent. For physical feasibility, we will assume that $W_c > W_d$ such that the aircraft has more fuel at the beginning of cruise than at the end of cruise.

Despite the availability of the optimal state-feedback airspeed, it is still a regular occurrence in the literature to assume a constant airspeed. This section will prove that it is suboptimal to fly at a constant airspeed. The proof will be done in two steps: first, an expression for the best constant airspeed will be derived; second, it will be shown that for $W_c > W_d$, the state-feedback solution endurance time is greater than the best constant airspeed solution.

Theorem 4. *For a turbojet in cruise, the constant airspeed which maximizes endurance is*

$$\bar{v}^* = \sqrt{\frac{2\sqrt{W_c W_d}}{\rho S} \sqrt{\frac{C_{D2}}{C_{D0}}}}$$

and the difference in endurance time between flying at the optimal state-feedback airspeed (49) and

the optimal constant airspeed is

$$\Delta J = J(v^*) - J(\bar{v}^*) = \frac{1}{S_{FC}\sqrt{C_{D0}C_{D2}}} \left(\frac{1}{2} \ln \left(\frac{W_c}{W_d} \right) - \tan^{-1} \left(\sqrt{\frac{W_c}{W_d}} \right) + \tan^{-1} \left(\sqrt{\frac{W_d}{W_c}} \right) \right)$$

and is strictly positive for $W_c > W_d$.

Proof. Let \bar{v} be some constant airspeed. It is possible to derive the total endurance time of an aircraft flown at speed \bar{v} by solving the differential equation

$$\dot{W} = \frac{dW}{dt} = -S_{FC}D(W, \bar{v}, \rho) \quad (51)$$

where drag D is defined in (12). Replacing (12) into (51) yields

$$\frac{dW}{dt} = -S_{FC} \left(\frac{1}{2} \rho S C_{D0} v^2 + \frac{2C_{D2}W^2}{\rho S v^2} \right) \quad (52)$$

Since altitude is constant, then the air density ρ is also constant, and therefore (52) is separable. Using the boundary conditions $W(t_c) = W_c$ and $W(t_d) = W_d$, (52) can be integrated to obtain the total endurance time in cruise $J(\bar{v})$

$$J(\bar{v}) = \int_{t_c}^{t_d} dt = -\frac{1}{S_{FC}} \int_{W_c}^{W_d} \left(\frac{1}{2} \rho S C_{D0} \bar{v}^2 + \frac{2C_{D2}W^2}{\rho S \bar{v}^2} \right)^{-1} dW \quad (53)$$

Solving the integral gives

$$J(\bar{v}) = \frac{1}{S_{FC}\sqrt{C_{D0}C_{D2}}} \left(\tan^{-1} \left(\frac{2W_c}{\rho S \bar{v}^2} \sqrt{\frac{C_{D2}}{C_{D0}}} \right) - \tan^{-1} \left(\frac{2W_d}{\rho S \bar{v}^2} \sqrt{\frac{C_{D2}}{C_{D0}}} \right) \right) \quad (54)$$

Next, we would like to determine the constant airspeed \bar{v} which maximizes (54). Without loss of generality, we will define the constant airspeed \bar{v} as

$$\bar{v} = \sqrt{\frac{2\bar{W}}{\rho S} \sqrt{\frac{C_{D2}}{C_{D0}}}} \quad (55)$$

which will allow us to instead solve for the optimal value of \bar{W} that maximizes (54). Replacing (55) into (54) yields

$$J(\bar{v}) = \frac{1}{S_{FC}\sqrt{C_{D0}C_{D2}}} \left(\tan^{-1} \left(\frac{W_c}{\bar{W}} \right) - \tan^{-1} \left(\frac{W_d}{\bar{W}} \right) \right) \quad (56)$$

The first order necessary condition for a maximum is that the first derivative of $J(\bar{v})$ with respect to \bar{W} be equal to zero

$$\frac{\partial J(\bar{W})}{\partial \bar{W}} = -\frac{1}{S_{FC}\sqrt{C_{D0}C_{D2}}} \left(\frac{W_c}{W_c^2 + \bar{W}^2} - \frac{W_d}{W_d^2 + \bar{W}^2} \right) = 0 \quad (57)$$

Since S_{FC} , C_{D0} , and C_{D2} are strictly positive, then the necessary condition in (57) is equivalent to

$$\frac{W_c}{W_c^2 + \bar{W}^2} - \frac{W_d}{W_d^2 + \bar{W}^2} = 0 \quad (58)$$

Expressing both terms over a common denominator gives

$$\frac{W_c(W_d^2 + \bar{W}^2) - W_d(W_c^2 + \bar{W}^2)}{(W_c^2 + \bar{W}^2)(W_d^2 + \bar{W}^2)} = 0 \quad (59)$$

Next, since the denominator is strictly positive, an expression for \bar{W}^2 can be found by isolating for \bar{W}^2 in the numerator

$$\bar{W}^2 = \frac{W_d W_c^2 - W_c W_d^2}{W_c - W_d} \quad (60)$$

Solving for \bar{W} yields

$$\bar{W} = \sqrt{W_c W_d} \quad (61)$$

which is the optimal value of \bar{W} that maximizes (56). Substituting (61) into (55) yields the optimal constant airspeed

$$\bar{v}^* = \sqrt{\frac{2\sqrt{W_c W_d}}{\rho S} \sqrt{\frac{C_{D0}}{C_{D2}}}} \quad (62)$$

To verify that (61) is a maximum, we can take the second derivative of (56), which is

$$\frac{\partial^2 J}{\partial \bar{W}^2} = \frac{1}{S_{FC}\sqrt{C_{D0}C_{D2}}} \left(\frac{2W_c\bar{W}}{(W_c^2 + \bar{W}^2)^2} - \frac{2W_d\bar{W}}{(W_d^2 + \bar{W}^2)^2} \right) \quad (63)$$

putting the terms within the brackets over the same common denominator yields

$$\frac{\partial^2 J}{\partial \bar{W}^2} = \frac{2\bar{W}}{S_{FC}\sqrt{C_{D0}C_{D2}}} \left(\frac{W_c (W_d^2 + \bar{W}^2)^2 - W_d (W_c^2 + \bar{W}^2)^2}{(W_c^2 + \bar{W}^2)^2 (W_d^2 + \bar{W}^2)^2} \right) \quad (64)$$

Since the left-hand multiplication term and the denominator of the term within the brackets are both positive, then the necessary condition is that the numerator be negative. The numerator can be expanded as

$$\begin{aligned} & W_c (W_d^2 + \bar{W}^2)^2 - W_d (W_c^2 + \bar{W}^2)^2 \\ &= W_c W_d^4 + 2W_c W_d^2 \bar{W}^2 + W_c \bar{W}^4 - W_c^4 W_d - 2W_c^2 W_d \bar{W}^2 - W_d \bar{W}^4 \end{aligned} \quad (65)$$

The terms can be grouped as

$$W_c W_d (W_d^3 - W_c^3) + 2W_c W_d \bar{W}^2 (W_d - W_c) + \bar{W}^4 (W_c - W_d) \quad (66)$$

Factoring the last two terms together yields

$$W_c W_d (W_d^3 - W_c^3) + (2W_c W_d \bar{W}^2 - \bar{W}^4) (W_d - W_c) \quad (67)$$

The first term is strictly negative since $W_d < W_c$. The second term is negative if

$$2W_c W_d \bar{W}^2 - \bar{W}^4 > 0 \quad (68)$$

which is equivalent to

$$\bar{W} < \sqrt{2W_c W_d} \quad (69)$$

Since \bar{W} is $\sqrt{W_c W_d}$, then (63) will be strictly negative and (61) is a global maximizer of (56).

Replacing (61) into (56) yields the best possible endurance time given the optimal constant airspeed (62)

$$J(\bar{v}^*) = \frac{1}{S_{FC}\sqrt{C_{D0}C_{D2}}} \left(\tan^{-1} \left(\sqrt{\frac{W_c}{W_d}} \right) - \tan^{-1} \left(\sqrt{\frac{W_d}{W_c}} \right) \right) \quad (70)$$

In order to compare the optimal state-feedback solution with the best possible constant airspeed solution, we will define ΔJ as the difference between the optimal solution given in (50) and the endurance time for optimal constant airspeed (70)

$$\Delta J = J^* - J(\bar{v}^*) = \frac{1}{S_{FC}\sqrt{C_{D0}C_{D2}}} \left(\frac{1}{2} \ln \left(\frac{W_c}{W_d} \right) - \tan^{-1} \left(\sqrt{\frac{W_c}{W_d}} \right) + \tan^{-1} \left(\sqrt{\frac{W_d}{W_c}} \right) \right) \quad (71)$$

Next, it must be shown that (71) is strictly positive to imply that the state-feedback solution is strictly superior. We will use the fact that when $W_c = W_d$ then (71) is zero, and then show that for any $W_c > W_d$, (71) will be strictly positive.

Replacing all instances of W_d by W_c in (71) it is clear that when $W_c = W_d$, (71) is zero. This shows that if there is no fuel to fly, then the endurance time will be zero regardless of the speed profile chosen. Next, it will be shown that (71) increases with W_c since its derivative is positive. The first derivative of (71) with respect to W_c is

$$\frac{\partial \Delta J}{\partial W_c} = \frac{1}{S_{FC}\sqrt{C_{D0}C_{D2}}} \left(\frac{1}{2W_c} - \frac{1}{2\sqrt{\frac{W_c}{W_d}}(W_c + W_d)} - \frac{\sqrt{\frac{W_d}{W_c}}}{2(W_c + W_d)} \right) \quad (72)$$

Rearranging the terms within the brackets yields

$$\frac{\partial \Delta J}{\partial W_c} = \frac{1}{2S_{FC}\sqrt{C_{D0}C_{D2}}} \left(\frac{\sqrt{W_c}(W_c + W_d) - 2W_c\sqrt{W_d}}{W_c(W_c + W_d)\sqrt{W_c}} \right) \quad (73)$$

Showing that (72) is positive is equivalent to showing that the numerator in (73) is positive. We start by writing

$$W_c^2 - 2W_cW_d + W_d^2 > 0 \quad (74)$$

which is strictly positive for $W_c \neq W_d$. Next, adding and subtracting $4W_cW_d$ gives

$$W_c^2 + 2W_cW_d + W_d^2 - 4W_cW_d > 0 \quad (75)$$

Moving the last term to the right-hand side and multiplying both sides by W_c yields

$$W_c(W_c^2 + 2W_cW_d + W_d^2) > 4W_c^2W_d \quad (76)$$

Taking the square root of both sides gives

$$\sqrt{W_c}(W_c + W_d) > 2W_c\sqrt{W_d} \quad (77)$$

Moving all terms to the left-hand side

$$\sqrt{W_c}(W_c + W_d) - 2W_c\sqrt{W_d} > 0 \quad (78)$$

which is equivalent to the numerator in (73) and shows that (72) is positive. Furthermore, since (71) increases monotonically with W_c for $W_c \neq W_d$, and crosses zero at $W_c = W_d$, then for any $W_c > W_d$ the state-feedback optimal control airspeed will perform better than the best constant airspeed (62).

□

Chapter 3

Maximum Endurance in Cruise

This chapter will present an optimal control approach to the problem of maximum endurance of fixed-wing aircraft in cruise. First, the problem will be solved using a unified energy-depletion model for fixed-wing aircraft, then it will be solved for specific aircraft configurations.

3.1 Assumptions and Models

In addition to Assumptions 2.1.1 to 2.1.4, the following assumptions will be made for steady flight in cruise

Assumption 3.1.1. *The aircraft flies below the drag divergence Mach number*

Assumption 3.1.2. *The aircraft experiences no lateral movement or forces*

Assumption 3.1.3. *The aircraft is in level cruise, i.e. $\gamma = 0$*

Assumption 3.1.4. *The aircraft is in steady (unaccelerated) flight*

Assumption 3.1.5. *The flight path angle γ and the angle of attack α are small such that $\cos \gamma \approx 1$ and $\sin \gamma \approx \gamma$ (and similarly for the angle of attack α)*

Assumption 3.1.6. *Specific fuel consumption is constant for turbojet and turboprop aircraft and depends only on airspeed for turbofan aircraft. Furthermore, the altitude effect on specific fuel consumption defined by (14) is small, i.e. $\delta(h) \approx 1$*

From Assumptions 3.1.3 to 3.1.5, dynamics (11) yields the following expression

$$T = D \quad (79)$$

From Assumption 3.1.3, the dynamics (8) become

$$\dot{x} = v + \omega \quad (80)$$

From Assumption 3.1.1, the drag will be modelled using the drag polar as

$$D = \frac{1}{2}\rho S C_{D0} v^2 + \frac{2C_{D2} W^2}{\rho S v^2} \quad (81)$$

where ρ is the air density, S is the wing area, W is the aircraft weight, C_{D0} is the parasitic drag coefficient and C_{D2} is the induced drag coefficient.

The energy dynamics will be generalized as

$$\dot{E} = -f(W, v, \rho) \quad (82)$$

for all aircraft, where the function f satisfies Assumption 3.1.7 and will be aircraft dependent.

Assumption 3.1.7. $f(W, v, \rho)$ is of class C^2 , is positive, has bounded derivative, and is strictly convex with respect to the airspeed v for $v > 0$

From Assumptions 3.1.6 to 3.1.6, specific fuel consumption will be approximated as

$$S_{FC} = \left(a + b \frac{v}{c} \right) \quad (83)$$

where the coefficient a is a positive constant and the coefficient b is given in Table 3.1 for each type of aircraft.

Table 3.1: Aircraft Dynamics Parameters

Engine Type	f , [J/s]	Fuel-Flow Coefficient, b
Turbojet	$eS_{FC}D(W, v, \rho)$	$b = 0$
Turbofan	$eS_{FC}D(W, v, \rho)$	$b > 0$
Turboprop	$eS_{FC}D(W, v, \rho)v$	$b = 0$
All-Electric	$D(W, v, \rho)v$	N/A

3.2 Maximum Endurance OCP

The endurance of an aircraft refers to the total flight time that the aircraft can stay aloft. Maximizing the total endurance time can be achieved by formulating and solving the problem using an optimal control framework.

Using this framework, the performance index J^* will be defined as the total flight time in cruise. The optimal control problem is

$$\begin{aligned}
 J^* &= \max_{v, t_d} \int_{t_c}^{t_d} dt \\
 \text{s.t.} \\
 \dot{x} &= v + \omega \\
 \dot{E} &= -f(W, v, \rho) \\
 E(t_c) &= E_c, E(t_d) = E_d \\
 h(t) &= h_c \\
 v &> 0 \\
 T &= D \\
 D &= \frac{1}{2}\rho S C_{D0} v^2 + \frac{2C_{D2}W^2}{\rho S v^2}
 \end{aligned} \tag{84}$$

where t_c is the time at top of climb, and t_d is the time at top of descent.

Remark 1. *The constraint that $v > 0$ ensures that the aircraft will only travel in one forward direction during flight. However, the true minimum airspeed is limited by the stall speed of the aircraft, as described in Section 2.1.3. In order to ensure feasibility of the solution, it should be verified that the resulting optimal airspeed for a particular aircraft is greater than its stall speed.*

3.3 Maximum Endurance Solution

This section provides a general solution to the maximum endurance problem (84).

Theorem 5. *The maximum endurance airspeed v^* is the unique maximizer of (84) and is determined by the first order necessary condition*

$$f_v(W, v, \rho) = 0 \quad (85)$$

and the maximum endurance time is

$$J^* = \int_{t_c}^{t_d} dt = - \int_{E_c}^{E_d} \frac{1}{f(W, v^*, \rho)} dE \quad (86)$$

Proof. The Hamiltonian is

$$H = 1 - J_E^* f(W, v, \rho) + J_x^* (v + \omega) \quad (87)$$

From Hamilton's equations, we have

$$\dot{J}_x^* = -H_x = 0 \quad (88)$$

which implies that $J_x^*(t)$ is constant with time. Since the final position $x(t_d)$ is free, the sensitivity to position at final time is

$$J_x^*(t_d) = 0 \quad (89)$$

which, coupled with (88), implies that

$$J_x^*(t) = 0 \quad \forall t \geq 0 \quad (90)$$

Therefore, the Hamiltonian (87) becomes

$$H = 1 - J_E^* f(W, v, \rho) \quad (91)$$

Since the Hamiltonian does not depend on time and the final time is free, we have

$$H^* = 1 - J_E^* f(W, v, \rho) = 0 \quad (92)$$

Solving for J_E^* gives

$$J_E^* = \frac{1}{f(W, v, \rho)} \quad (93)$$

Since f is positive from assumption 3.1.7, the costate J_E^* is also positive. The necessary condition in v is

$$H_v = -J_E^* f_v(W, v, \rho) = 0 \quad (94)$$

From $J_E^* > 0$, the necessary condition (94) is equivalent to

$$f_v(W, v, \rho) = 0 \quad (95)$$

From assumption 3.1.7 the necessary condition (95) will have one global maximizer v^* , which is defined as $f_v(W, v^*, \rho) = 0$.

The second order sufficient condition in v is

$$H_{vv} = -J_E^* f_{vv}(W, v, \rho) < 0 \quad (96)$$

which is satisfied from $J_E^* > 0$ and from the strict convexity of f under assumption 3.1.7.

Finally, the total endurance time can be found by solving the differential equation

$$\dot{E} = \frac{dE}{dt} = -f(W, v^*, \rho) \quad (97)$$

from top of climb to top of descent and evaluated at $v = v^*$. Therefore the total endurance time is

$$J^* = \int_{t_c}^{t_d} dt = - \int_{E_c}^{E_d} \frac{1}{f(W, v^*, \rho)} dE \quad (98)$$

□

3.4 Solved Examples

The results of Section 3.3 are readily adaptable to different engine configurations. This section provides specific solutions for different aircraft configurations: turbojet, turbofan, turboprop, and all-electric. A summary of the results is provided in Section 3.6.

3.4.1 Turbojet

The maximum endurance problem of a turbojet was already solved in [27]. However, the same results can be found using the proposed methodology in 3.3.

From Table 3.1, the energy dynamics of a turbojet are

$$\dot{E} = -f_{jet} = -eS_{FC}D(W, v, \rho) \quad (99)$$

Multiplying the first order necessary condition in Table 3.3 by v^3 yields the following bi-quadratic in v

$$\rho S C_{D0} v^4 - \frac{4C_{D2}W^2}{\rho S} = 0 \quad (100)$$

Solving for v yields the maximum endurance airspeed for a turbojet

$$v^* = \sqrt{\frac{2W}{\rho S} \sqrt{\frac{C_{D2}}{C_{D0}}}} \quad (101)$$

Replacing (99) into (96), the second order necessary condition for a turbojet is

$$H_{vv} = -J_W^* e S_{FC} \left(\rho S C_{D0} + \frac{12 C_{D0} W^2}{\rho S v^4} \right) < 0 \quad (102)$$

which holds since $J_W^* > 0$, $e > 0$, $S_{FC} > 0$, $\rho > 0$, $S > 0$, $C_{D0} > 0$, and $C_{D2} > 0$.

Finally, the maximum endurance time can be found by solving the integral (98), which yields

$$J^* = \frac{1}{2 S_{FC} \sqrt{C_{D2} C_{D0}}} \ln \left(\frac{W_c}{W_d} \right) \quad (103)$$

and is the well-known Breguet equation for maximum range.

3.4.2 Turbofan

The maximum endurance problem can be solved following the procedure in Section 3.3. From Table 3.1, the energy dynamics of a turbofan are

$$\dot{E} = -f_{fan} = -e S_{FC} D(W, v, \rho) \quad (104)$$

Multiplying the first order necessary condition in Table 3.3 by v^3 yields the following fifth order polynomial in v

$$q(v) = \frac{3 b C_{D0} \rho S}{2 c} v^5 + C_{D0} \rho S v^4 - \frac{2 b W^2 C_{D2}}{c \rho S} v - \frac{4 W^2 C_{D2}}{\rho S} = 0 \quad (105)$$

From Descartes rule of signs, there is one real root of q which is the maximum endurance airspeed of a turbofan. There is no analytical expression to determine the root of the necessary condition (105). Therefore, the next section will develop an approximate analytical solution to (105) based on Newton's method.

Replacing (104) into (96), the second order necessary condition for a turbofan is

$$H_{vv} = -J_W^* e a \left(\frac{3 b \rho S C_{D0} v}{c} + \frac{4 b C_{D2} W^2}{c \rho S v^3} + \rho S C_{D0} + \frac{12 C_{D2} W^2}{\rho S v^4} \right) < 0 \quad (106)$$

which holds since $J_W^* > 0$, $e > 0$, $a > 0$, $b > 0$, $c > 0$, $\rho > 0$, $S > 0$, $C_{D0} > 0$, $C_{D2} > 0$, and

$v > 0$.

Approximate Analytical Solution using Newton's Method

There is no analytic expression for finding the roots of a fifth order polynomial of the form (105). Therefore, numerical methods must be used to solve for the optimal airspeed. However, an approximate analytical solution can be found using the first iteration of Newton's method if an initial seed can be chosen which is sufficiently close to the optimal solution.

For low by-pass ratios, a turbofan engine can be approximated as a turbojet engine. Therefore, one would expect that a good initial seed could be the maximum endurance solution of a turbojet (101). Using the maximum endurance airspeed for a turbojet, v_{jet}^* (101) as the initial seed of Newton's method, we obtain an approximate solution of the maximum endurance airspeed. In the following section error bounds will be derived to validate the selection of the initial seed. The approximate solution will be denoted \tilde{v}^* , and is defined as

$$v^* \approx \tilde{v}^* = v_{jet}^* - \frac{q(v_{jet}^*)}{q'(v_{jet}^*)} \quad (107)$$

where

$$q'(v) = \frac{15}{2} \frac{bC_{D0}\rho S}{c} v^4 + 4C_{D0}\rho S v^3 - \frac{2bW^2 C_{D2}}{c\rho S} \quad (108)$$

and

$$\frac{q(v)}{q'(v)} = \frac{3bC_{D0}\rho^2 S^2 v^5 - 4bW^2 C_{D2} v + 2C_{D0}\rho^2 S^2 c v^4 - 8W^2 C_{D2} c}{15bC_{D0}\rho^2 S^2 v^4 - 4bW^2 C_{D2} + 8C_{D0}\rho^2 S^2 c v^3} \quad (109)$$

Newton's method is only valid for $q'(v_{jet}^*) \neq 0$. Evaluating $q'(v_{jet}^*)$ yields

$$q'(v_{jet}^*) = 56bC_{D2}W^2 + 8c\sqrt{8\rho SW^3 \sqrt{C_{D2}^3 C_{D0}}} > 0 \quad (110)$$

This constraint is verified since all of the coefficients and weight are strictly positive. Furthermore, evaluating $q(v_{jet}^*)$ yields

$$q(v_{jet}^*) = 4W^2 \frac{b}{c} \frac{C_{D2}}{\rho S} \sqrt{\frac{2W}{\rho S} \sqrt{\frac{C_{D2}}{C_{D0}}}} \quad (111)$$

Replacing (101), (110), and (111) into (107) gives

$$\tilde{v}_{fan}^* = \sqrt{\frac{2W}{\rho S} \sqrt{\frac{C_{D2}}{C_{D0}}}} \left(1 - \frac{\frac{4bW^2 C_{D2}}{c\rho S}}{56bW^2 C_{D2} + 8c\sqrt{8\rho S W^3 \sqrt{C_{D2}^3 C_{D0}}}} \right) \quad (112)$$

which is the approximate solution for the maximum endurance speed of a turbofan. Note that when $b = 0$, the expression for S_{FC} becomes constant in v , as in the case of a turbojet. Furthermore, when $b = 0$, then (112) reduces to v_{jet}^* in (101), as expected.

Upper Error Bound

This section will derive upper error bounds for the proposed approximate solution (112). The error bounds will be derived following Miel's work [56], which is also summarized in [57].

The following lemma is adapted from Theorem 2.1 in [58] and is used to define an interval containing the optimal solution.

Lemma 6. *Let $V = \mathbb{R}$, $q(v) \in C^2$, $v_0 \in V$, $q'(v_0) \neq 0$, $\sigma_0 = -q(v_0)/q'(v_0)$, $\eta = |\sigma_0|$, and*

$$I = \begin{cases} [v_0, v_0 + 2\sigma_0] & \text{if } \sigma_0 \geq 0 \\ [v_0 + 2\sigma_0, v_0] & \text{if } \sigma_0 < 0 \end{cases} \quad (113)$$

then $q(v) = 0$ has a unique solution v^ in I .*

The following lemma is adapted from Theorem 4.1 from [56], which provides error bounds on Newton-type iterative methods, and is valid for n iterations. However, the lemma is modified to consider only the first iteration.

Lemma 7. *Let $V = \mathbb{R}$, $q(v) \in C^2$, $v_0 \in V$, $q'(v_0) \neq 0$, $g_1 = |q(v_0)/q'(v_0)|$, $g_2 = |1/q'(v_0)|$.*

Define

$$K = \sup |q''(v)| \in I \quad (114)$$

where I is defined in (113). Then, if

$$h = Kg_1g_2 \leq \frac{1}{2} \quad (115)$$

the smallest possible error bound on the first iteration of Newton's method

$$v_1 = v_0 - \frac{q(v_0)}{q'(v_0)} \quad (116)$$

is given by

$$|v^* - v_1| \leq \left(\frac{1 - \sqrt{1 - 2h}}{1 + \sqrt{1 - 2h}} \right) \frac{f(v_0)}{f'(v_0)} \quad (117)$$

Theorem 8. Let $v_0 = v_{jet}^*$ be the initial seed of the first iteration of Newton's method, and let $q \in C^3$. Under the assumptions of lemmas 2 and 3, the approximate solution (112) has a maximum error given by

$$|v_{fan}^* - \tilde{v}_{fan}^*| \leq \left(\frac{1 - \sqrt{1 - 2h}}{1 + \sqrt{1 - 2h}} \right) \frac{q(v_{jet}^*)}{q'(v_{jet}^*)} \quad (118)$$

where h is given by

$$h = \frac{|q''(v_{jet}^*)q(v_{jet}^*)|}{[q'(v_{jet}^*)]^2} \leq \frac{1}{2} \quad (119)$$

Proof. Define

$$\sigma_0 = -\frac{q(v_{jet}^*)}{q'(v_{jet}^*)} \quad (120)$$

Since expressions (111) and (110) are strictly positive, σ_0 will be strictly negative. Therefore, we define the interval I containing a unique solution to (105) as

$$I = [v_{jet}^* + 2\sigma_0, v_{jet}^*] \quad (121)$$

Define

$$g_1 = |\sigma_0|, g_2 = \left| \frac{1}{q'(v_{jet}^*)} \right| \quad (122)$$

The second derivative of $q(v)$ is

$$q''(v) = \frac{30bC_{D0}\rho S}{c}v^3 + 12C_{D0}\rho Sv^2 > 0 \quad (123)$$

which implies that $q''(v) = |q''(v)|$, and third derivative of $q(v)$ is

$$q'''(v) = \frac{90bC_{D0}\rho S}{c}v^2 + 24C_{D0}\rho Sv > 0 \quad (124)$$

Since $q''(v) > 0$ and $q'''(v) > 0$, then it is clear that $q''(v)$ is positive and increases with v . Therefore, the value of $v \in I$ which maximizes (123) is the maximum value of $v \in I$, which from (121) is v_{jet}^* . Therefore

$$K = q''(v_{jet}^*) \quad (125)$$

and

$$h = \frac{\left| q''(v_{jet}^*)q(v_{jet}^*) \right|}{[q'(v_{jet}^*)]^2} \leq \frac{1}{2} \quad (126)$$

From Lemma 7, the error of the approximate solution in (112) is bounded by

$$|v_{fan}^* - \tilde{v}_{fan}^*| \leq \left(\frac{1 - \sqrt{1 - 2h}}{1 + \sqrt{1 - 2h}} \right) \frac{q(v_{jet}^*)}{q'(v_{jet}^*)} \quad (127)$$

□

3.4.3 Turboprop

Once again, the maximum endurance problem of a turboprop can be solved using the procedure outlined in Section 3.3. From Table 3.1, the energy dynamics of a turbojet are

$$\dot{E} = -f_{prop} = -eS_{FC}D(W, v, \rho)v \quad (128)$$

Multiplying the first order necessary condition in Table 3.3 by v^3 yields the following bi-quadratic in v

$$\frac{3}{2}\rho SC_{D0}v^4 - \frac{2C_{D2}W^2}{\rho S} = 0 \quad (129)$$

Solving for v yields the maximum endurance airspeed for a turboprop

$$v^* = \sqrt{\frac{2W}{\rho S} \sqrt{\frac{C_{D2}}{3C_{D0}}}} \quad (130)$$

Replacing (128) into (96), the second order necessary condition for a turboprop is

$$H_{vv} = -J_W^* S_{FC} \left(\frac{3}{2}\rho SC_{D0} + \frac{12C_{D2}W^2}{\rho S v^4} \right) < 0 \quad (131)$$

which holds since $J_W^* > 0$, $e > 0$, $S_{FC} > 0$, $\rho > 0$, $S > 0$, $C_{D0} > 0$, and $C_{D2} > 0$.

Finally, the maximum endurance time can be found by solving the integral (98), which yields

$$J^* = \frac{1}{2S_{FC}} \left(\sqrt{\frac{2C_{D0}C_{D2}}{3\rho S} \sqrt{\frac{C_{D2}}{3C_{D0}}}} \right)^{-1} \left(\frac{1}{\sqrt{W_d}} - \frac{1}{\sqrt{W_c}} \right) \quad (132)$$

Sensitivity to Altitude

Since the total endurance time (132) is differentiable with respect to ρ , the sensitivity of endurance time with respect to air density J_ρ^* can be obtained as

$$J_\rho^* = \frac{\partial J^*}{\partial \rho} = \frac{1}{4S_{FC}\sqrt{\rho}} \left(\sqrt{\frac{2C_{D0}C_{D2}}{3S} \sqrt{\frac{C_{D2}}{3C_{D0}}}} \right)^{-1} \left(\frac{1}{\sqrt{W_d}} - \frac{1}{\sqrt{W_c}} \right) \quad (133)$$

Since $\left(\frac{1}{\sqrt{W_c}} - \frac{1}{\sqrt{W_d}} \right) > 0$ for $W_c > W_d$, and $\rho > 0$, $S_{FC} > 0$, $S > 0$, $C_{D0} > 0$, and $C_{D2} > 0$, then $J_\rho^* > 0$. Furthermore, since the objective is to maximize the endurance J^* , then a positive sensitivity J_ρ^* implies that the aircraft should be flown at the highest possible air density in order

to maximize J^* . Because air density decreases with altitude, this translates to flying at the lowest allowable altitude.

3.4.4 All-Electric

The maximum endurance problem of an all-electric aircraft in cruise was already solved in [29]. However, the same results can be found using the proposed methodology from Section 3.3.

From Table 3.1, the energy dynamics of an all-electric aircraft are

$$\dot{E} = -f_{elec} = -D(W, v, \rho)v \quad (134)$$

Multiplying the first order necessary condition in Table 3.3 by v^3 yields the following bi-quadratic in v

$$\frac{3}{2}\rho S C_{D0} v^4 - \frac{2C_{D2}W^2}{\rho S} = 0 \quad (135)$$

Solving for v yields the maximum endurance airspeed for a turboprop

$$v^* = \sqrt{\frac{2W}{\rho S} \sqrt{\frac{C_{D2}}{3C_{D0}}}} \quad (136)$$

Note that in the case of the all-electric aircraft the weight is constant and therefore the optimal airspeed (136) is constant for constant altitude.

From (134) and (96), the second order necessary condition for an all-electric aircraft is

$$H_{vv} = -J_E^* \left(\frac{3}{2}\rho S C_{D0} + \frac{12C_{D2}W^2}{\rho S v^4} \right) < 0 \quad (137)$$

which holds since $J_E^* > 0$, $\rho > 0$, $S > 0$, $C_{D0} > 0$, and $C_{D2} > 0$.

Finally, the maximum endurance time can be found by solving the integral (98), which yields

$$J^* = \frac{3^{3/4}(Q_c - Q_d)U\sqrt{\rho S}}{2^{5/2}W^{3/2}C_{D0}^{3/4}C_{D2}^{1/4}} \quad (138)$$

which is identical to the results presented in [29].

Sensitivity to Altitude

Since the total endurance time (138) is differentiable with respect to ρ , the sensitivity of endurance time with respect to air density J_ρ^* can be obtained as

$$J_\rho^* = \frac{3^{3/4}(Q_c - Q_d)U\sqrt{S}}{2^{7/2}W^{3/2}C_{D0}^{3/4}C_{D2}^{1/4}\sqrt{\rho}} \quad (139)$$

Since $Q_c - Q_d > 0$ for $Q_c > Q_d$, and $\rho > 0$, $S > 0$, $C_{D0} > 0$, and $C_{D2} > 0$, then $J_\rho^* > 0$. Furthermore, since the objective is to maximize the endurance J^* , then a positive sensitivity J_ρ^* implies that the aircraft should be flown at the highest possible air density in order to maximize J^* . Because air density decreases with altitude, this translates to flying at the lowest allowable altitude.

3.5 Aircraft Configurations

3.5.1 Aircraft Parameters

A summary of the aircraft parameters used for the simulations is provided in Table 3.2. The data for the Boeing 737 is taken from [59, 27], the data for the King Air 350 is taken from [22, 60], and the data for the Airbus E-Fan is taken from [61, 8, 29].

3.5.2 Turbojet

Figure 3.1 shows the optimal airspeed profile as a function of aircraft weight at cruising altitudes of 3,000 m and 11,000 m.

3.5.3 Turbofan

In order to validate the suboptimal control law in (112), it was compared to the exact solution of the quintic in (105). The exact solution was found using the root finder `vpasolve` in Matlab. The solver returns a solution accurate to 32 significant figures [62]. Therefore, the Matlab solver is

¹Turbofan approximated as a turbojet

Table 3.2: Summary of Aircraft Parameters

	Turbojet	Turbofan	Turboprop	All-Electric
Example aircraft	Boeing 737 ¹	Boeing 737	King Air 350	Airbus E-Fan
Wing area, S	125 m ²	125 m ²	26.75 m ²	10 m ²
Induced drag coefficient, C_{D0}	0.020	0.020	0.0185	0.025
Parasitic drag coefficient, C_{D2}	0.055	0.055	0.0263	0.039
Specific fuel consumption, S_{FC}	1.2407×10^{-4} 1/s	N/A	1.5174×10^{-6} 1/m	N/A
Fuel flow coefficient, a	N/A	1.0737×10^{-5} 1/s	N/A	N/A
Fuel flow coefficient, b	N/A	0.9045	N/A	N/A
Battery voltage, U	N/A	N/A	N/A	250 V

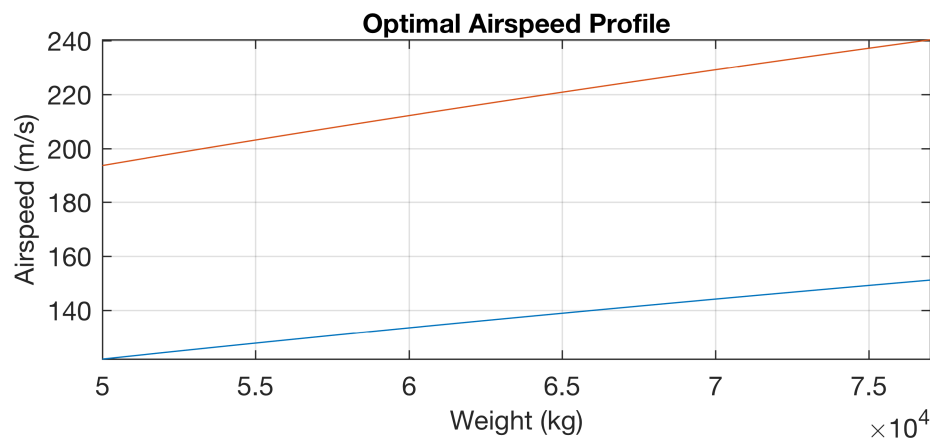


Figure 3.1: Comparison of Maximum Endurance Airspeed

assumed to have an error close to zero. The speeds were compared for weights ranging from 50,000 kg to 77,000 kg.

Figure 3.2 shows a comparison between the proposed control law given in (112) and the optimal solution. It can be seen that the proposed solution is very close to the optimal solution.

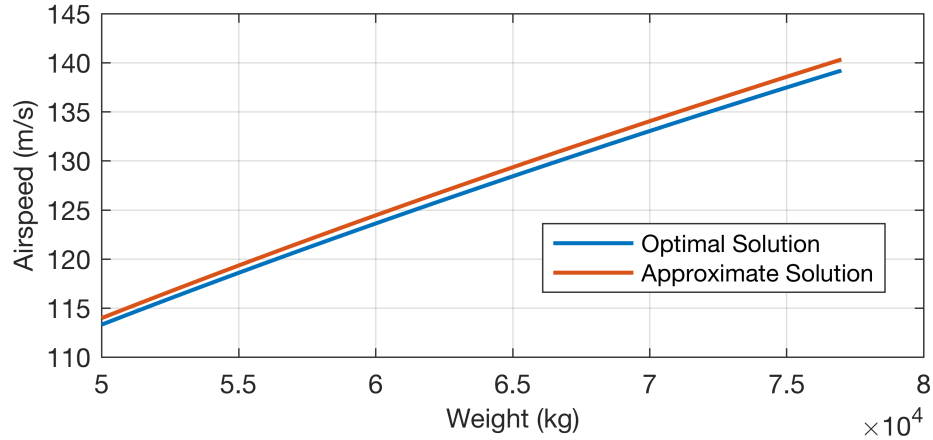


Figure 3.2: Comparison of Maximum Endurance Airspeed

Figure 3.3 shows the absolute error between the optimal solution and the suboptimal solution for airspeed. The error increases with weight. However, even at the maximum take-off weight of the aircraft, the error is still only 1.1242 m/s (or 0.8076%).

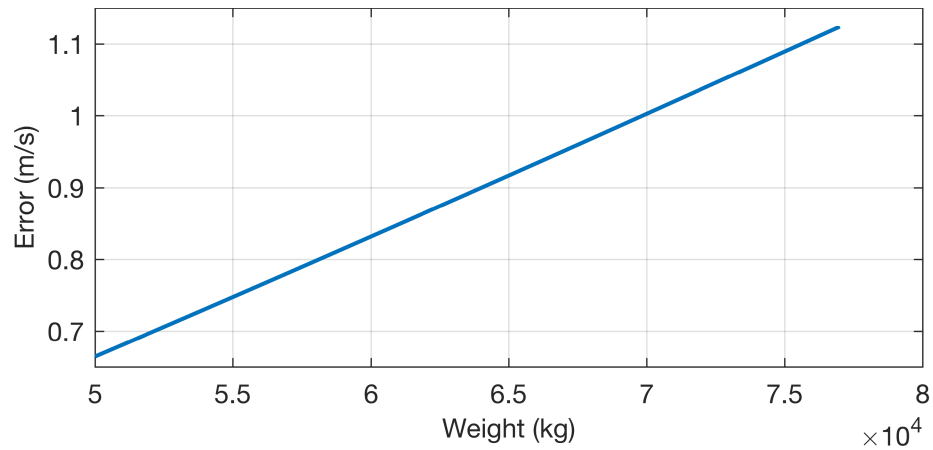


Figure 3.3: Error Analysis

Figures 3.4 and 3.5 show the percent error as a function of weight, plotted along with the error upper bound in (118) for altitudes of 10,000 ft and 30,000 ft, respectively. The maximum error of

the approximate solution is therefore bounded by around 1.43% in the worst case scenario (which is maximum altitude and maximum weight). In reality, the algorithm has a slightly better performance with a maximum error of 1.29% at maximum weight and altitude.

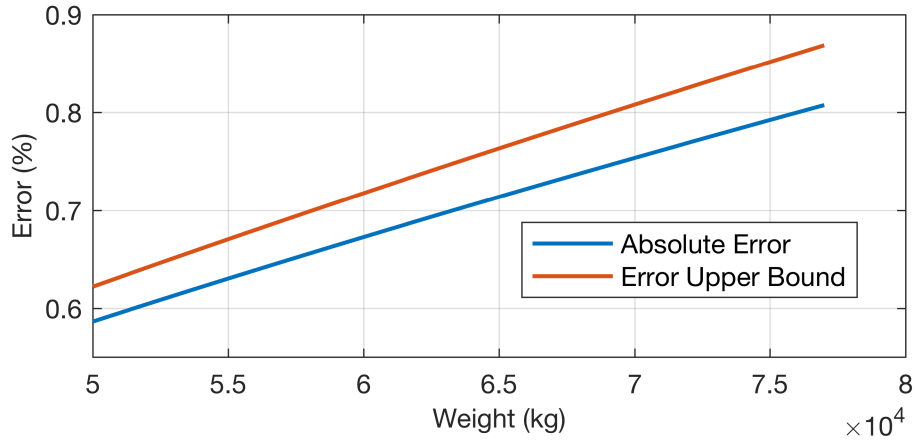


Figure 3.4: Error Upper Bound at 10,000 ft

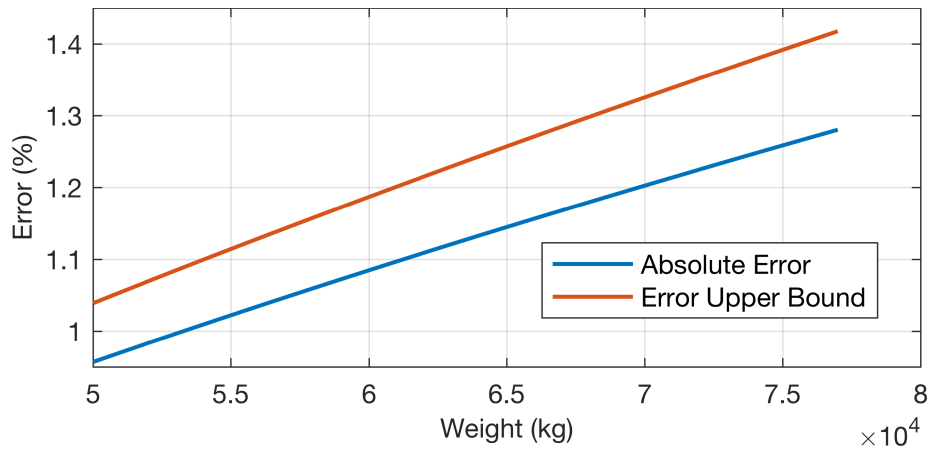


Figure 3.5: Error Upper Bound at 30,000 ft

Figures 3.6 and 3.7 show the the optimal solution for both the turbojet and the turbofan, as well as the approximate solution, at 10,000 ft and 30,000 ft respectively. The figures illustrate how the optimal turbofan airspeed is close to the turbojet solution, and validates the initial seed selection for the approximate solution using Newton’s method.

At TRU Simulation + Training, a flight simulator for the Boeing 737 was used to compare the turbofan maximum endurance solution with what is currently being implemented. The Boeing

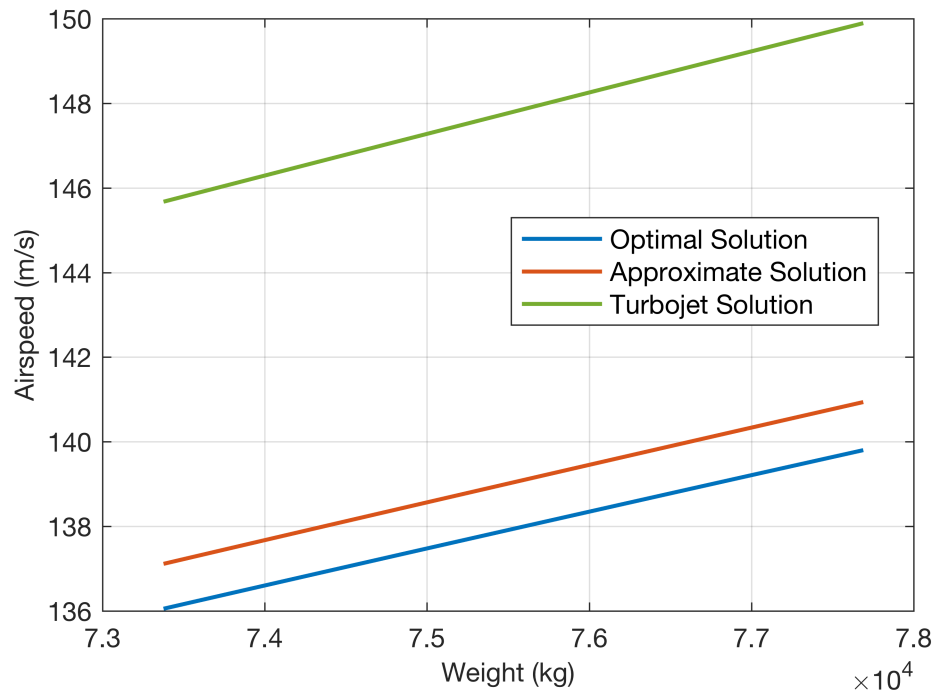


Figure 3.6: Comparison of Different Engine Configurations at 10,000 ft

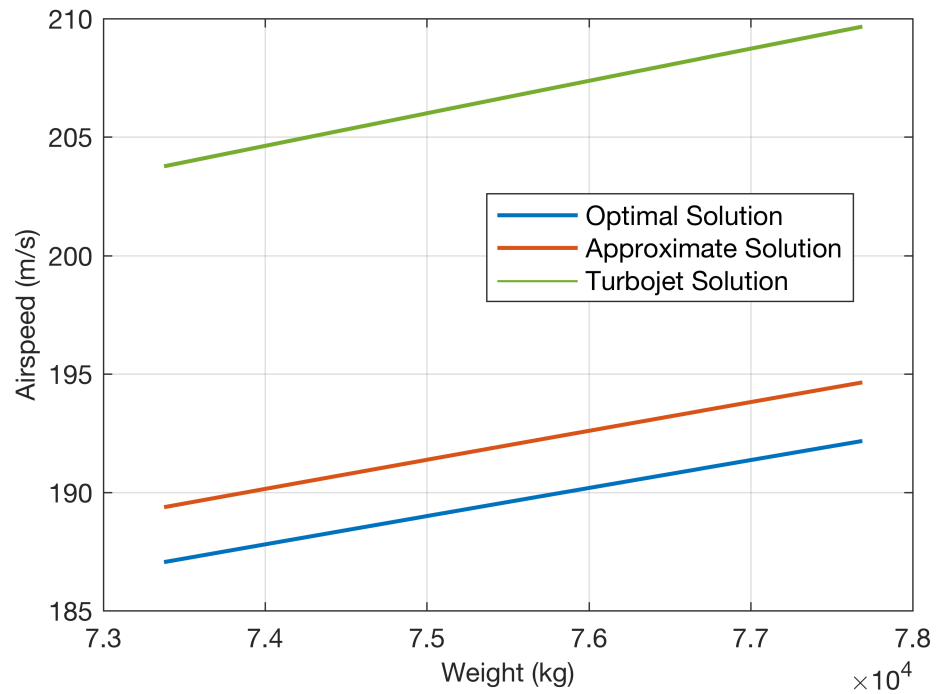


Figure 3.7: Comparison of Different Engine Configurations at 30,000 ft

737 FMS has several performance modes available, namely the HOLD performance mode, which attempts to maximize the endurance of the aircraft. During a HOLD procedure, the aircraft will follow a racetrack pattern above a given waypoint, and fly at an airspeed that maximizes endurance.

Figure 3.8 shows a plot of the FMS endurance airspeed versus the approximate and optimal control laws for varying weights. The FMS endurance speed was obtained by running a flight simulator equipped with an actual Boeing 737 FMS at TRU Simulation + Training. The optimal solution and approximate solution were calculated using the same initial conditions as the FMS simulation. From the graph, it is clear that the approximate solution is closer to the optimal solution than the FMS solution, which implies that (112) is a reasonable approximate solution and possibly an improvement on the FMS selected airspeed.

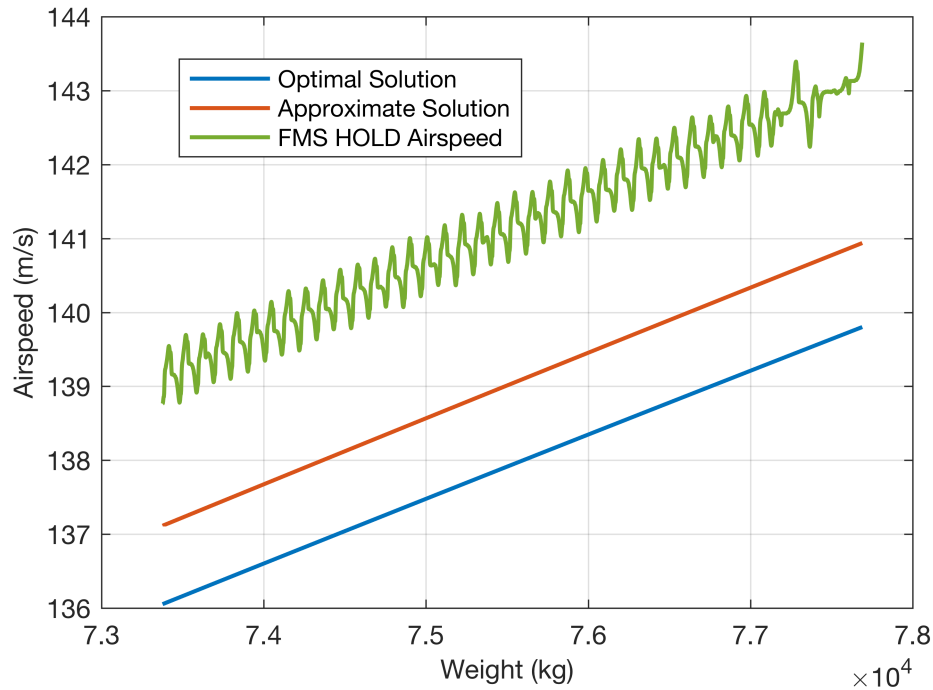


Figure 3.8: Comparison of Boeing 737 FMS

3.5.4 Turboprop

Figure 3.9 shows the optimal airspeed profile as a function of aircraft weight at cruising altitudes of 3,000 m and 11,000 m. Figure 3.10 shows that the sensitivity to air density is positive for the

range of altitudes simulated (3,000 m to 11,000 m). The air density at each altitude was modelled using the International Standard Atmosphere model (2). Figure 3.11 shows the total endurance time as a function of altitude. At a cruising altitude of 11,000 m, the total endurance time was 10.86 hours. However, at a cruising altitude of 3,000 m, the total endurance time was 17.26 hours (an increase of 58.9 %). This illustrates how sensitive the endurance time is to cruising altitude. An optimal strategy would therefore be to fly the aircraft at the lowest allowable altitude.

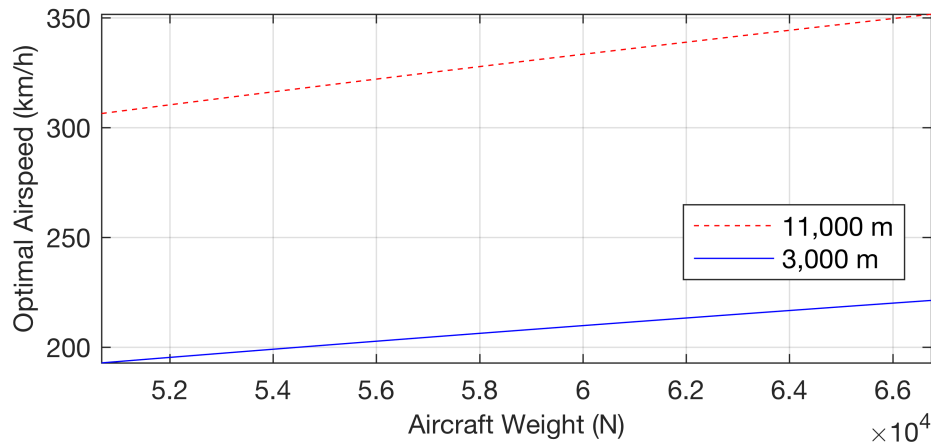


Figure 3.9: Optimal Airspeed Profiles

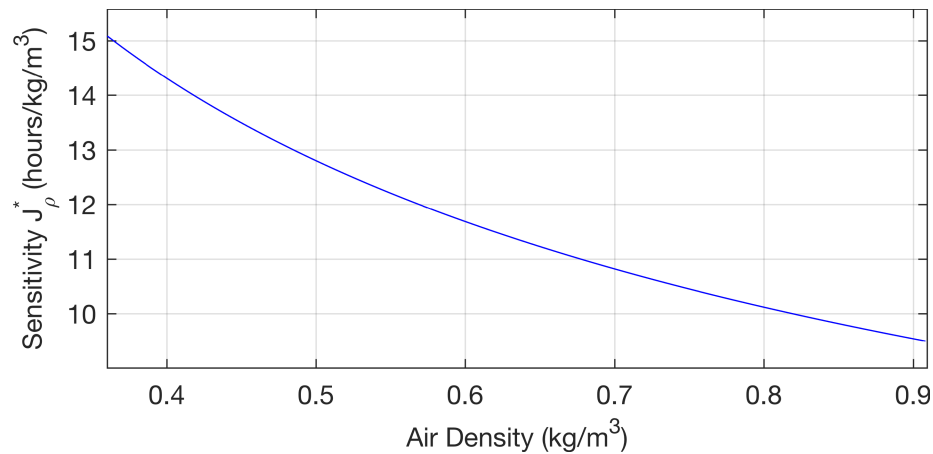


Figure 3.10: Sensitivity of Endurance to Air Density

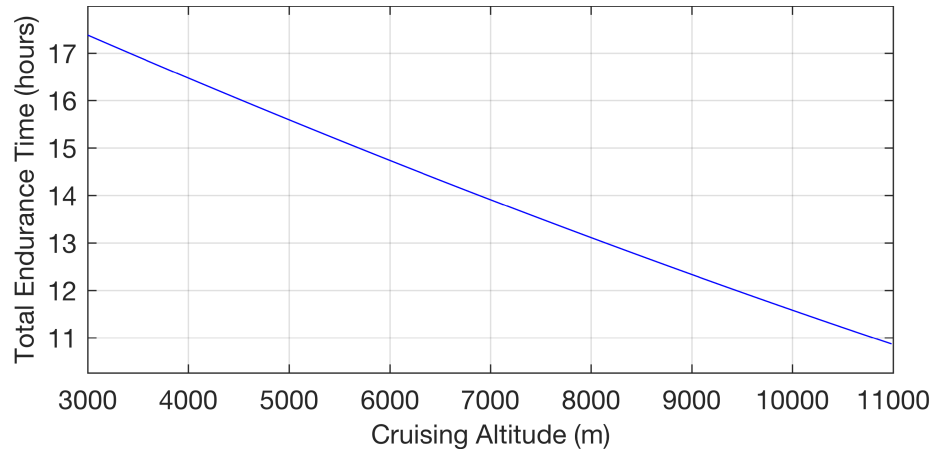


Figure 3.11: Maximum Endurance as a Function of Cruising Altitude

3.5.5 All-Electric

The optimal airspeed for the all-electric aircraft is constant. At 3,000 m, the optimal airspeed was 30.54 m/s, and at 11,000 m it was 48.56 m/s.

Figure 3.12 shows that the sensitivity to air density is positive for the range of altitudes simulated (sea level to 11,000 m). The air density at each altitude was modelled using the International Standard Atmosphere model (2). Figure 3.13 shows the total endurance time as a function of altitude and illustrates how the endurance is very sensitive to cruising altitude. An optimal strategy would therefore be to fly the aircraft at the lowest allowable altitude.

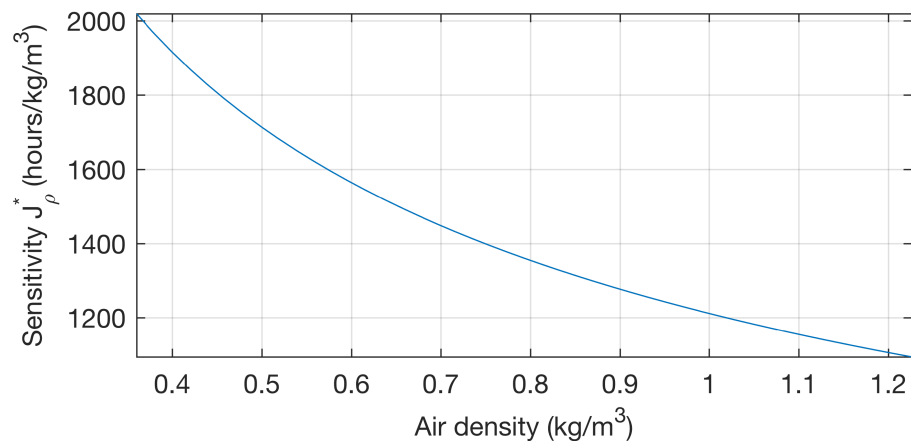


Figure 3.12: Sensitivity of Endurance to Air Density

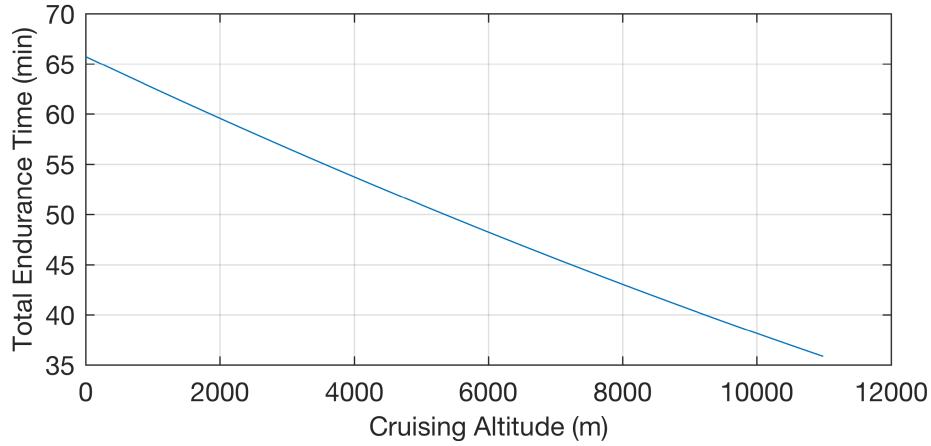


Figure 3.13: Maximum Endurance as a Function of Cruising Altitude

3.6 Summary

A summary of the results for each engine is given in Table 3.3.

Table 3.3: Maximum Endurance for Different Aircraft

Engine Type	Necessary Condition, $f_v = 0$	Optimal Airspeed, v^*
Turbojet	$\rho S C_{D0} v - \frac{4C_{D2} W^2}{\rho S v^3} = 0$	$\sqrt{\frac{2W}{\rho S}} \sqrt{\frac{C_{D2}}{C_{D0}}}$
Turbofan	$\frac{3}{2} \frac{bC_{D0} \rho S}{c} v^2 + C_{D0} \rho S v - \frac{2bW^2 C_{D2}}{c \rho S v^2} - \frac{4W^2 C_{D2}}{\rho S v^3} = 0$	No analytic solution ²
Turboprop	$\frac{3}{2} \rho S C_{D0} v - \frac{2C_{D2} W^2}{\rho S v^3} = 0$	$\sqrt{\frac{2W}{\rho S}} \sqrt{\frac{C_{D2}}{3C_{D0}}}$
All-Electric	$\frac{3}{2} \rho S C_{D0} v - \frac{2C_{D2} W^2}{\rho S v^3} = 0$	$\sqrt{\frac{2W}{\rho S}} \sqrt{\frac{C_{D2}}{3C_{D0}}}$

A comparison of the maximum airspeeds obtained in the simulations with the maximum cruising airspeeds of the example aircraft is given in Table 3.4 and shows that the resulting solutions do not exceed the allowable speeds. The maximum airspeeds for each aircraft are taken from [60, 63, 64].

²Approximate analytical solution provided in Section 3.4.2

Table 3.4: Optimal Airspeed Feasibility

Engine Type	Maximum Simulated Airspeed	Maximum Cruising Airspeed
Turbojet	752.4 km/h	833 km/h
Turbofan	691.9 km/h	833 km/h
Turboprop	350.0 km/h	578 km/h
All-Electric	174.8 km/h	220 km/h

Neither the total endurance nor the optimal airspeed profiles depend on the wind speed ω . This implies that the total endurance does not depend on wind speed. This result was expected since the final position is free. However, while the airspeed does not depend on the wind speed, the ground speed and final position will depend on ω .

Chapter 4

Maximum Cruise Endurance over Climb, Cruise, and Descent

This chapter will present a hybrid optimal control approach to the problem of maximum endurance of fixed-wing aircraft over climb, cruise, and descent. First, the problem will be solved using a unified energy-depletion model for fixed-wing aircraft, then it will be solved for specific aircraft configurations.

4.1 Assumptions and Models

In addition to Assumptions 2.1.1 to 2.1.4 for the all-electric battery model, the following assumptions will be made

Assumption 4.1.1. *The aircraft flies below the drag divergence Mach number*

Assumption 4.1.2. *The aircraft experiences no lateral movement or forces*

Assumption 4.1.3. *The aircraft follows a flight path which includes a climb segment ($\gamma > 0$), a level cruise segment ($\gamma = 0$), and a descent segment ($\gamma < 0$)*

Assumption 4.1.4. *The aircraft is in steady (unaccelerated) flight*

Assumption 4.1.5. *The flight path angle γ and the angle of attack α are small such that $\cos \gamma \approx 1$ and $\sin \gamma \approx \gamma$ (and similarly for the angle of attack α)*

Assumption 4.1.6. *Specific fuel consumption is constant for turbojet and turboprop aircraft and depends only on airspeed for turbofan aircraft. Furthermore, the altitude effect on specific fuel consumption defined by (14) is small, i.e. $\delta(h) \approx 1$*

Assumption 4.1.7. *Only the head-wind and tail-wind will be considered (vertical and cross-winds are ignored)*

Assumption 4.1.8. *The aircraft thrust is bounded by $T_{idle} \leq T \leq T_{max}(h)$*

From Assumption 4.1.6, specific fuel consumption will be approximated as

$$S_{FC} = \left(a + b \frac{v}{c} \right) \quad (140)$$

where the coefficient a is a positive constant and the coefficient b is given in Table 4.1 for each type of aircraft.

Using Assumption 4.1.5, the dynamics (8) become

$$\dot{x} = v + \omega \quad (141)$$

From Assumptions 4.1.4 and 4.1.5, dynamics (11) yield the following expression

$$T - D - W\gamma = 0 \quad (142)$$

Using Assumption 4.1.5 and substituting γ from (142) into (9) yields

$$\dot{h} = \frac{v(T - D)}{W} \quad (143)$$

The problem will be modelled using a hybrid optimal control framework. The hybrid system consists of: control inputs (v and T), continuous states (x , W , and h), and discrete states (climb, cruise, and descent). A hybrid automaton of the switched system for the three phases of flight is given in Figure 4.1.

The superscript notation $^{(q)}$ will be used to indicate the discrete state of the system. From Assumption 4.1.3 the aircraft will experience two switches: from climb to cruise, and then from

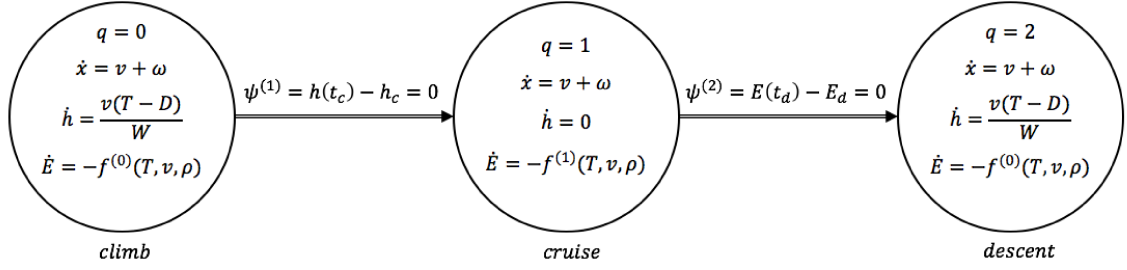


Figure 4.1: Hybrid Automaton

cruise to descent. The discrete states will be defined as

$$q = \begin{cases} 1 & \text{for climb } t_0 < t < t_c \\ 2 & \text{for cruise } t_c < t < t_d \\ 3 & \text{for descent } t_d < t < t_f \end{cases} \quad (144)$$

where t_0 is initial time, t_c is the time at top of climb, t_d is the time at top of descent, and t_f is final time. The dynamics in altitude for the switched system will therefore be described by

$$\dot{h} = \begin{cases} 0 & \text{for } t_c \leq t \leq t_d \\ \frac{v(T-D)}{W} & \text{otherwise} \end{cases} \quad (145)$$

The equations that relate fuel to energy and charge to energy from Section 2.1.7 will be used to generalize the dynamics of the system in terms of energy per unit time. From Assumption 4.1.3, and using the hybrid optimal control framework, the states of flight will be defined as

$$\dot{E} = \begin{cases} -f^{(1)}(W, v, \rho) & \text{for } t_c \leq t \leq t_d \\ -f^{(0)}(T, v, \rho) & \text{otherwise} \end{cases} \quad (146)$$

for all aircraft, where the function f satisfies Assumption 4.1.9 and will be aircraft dependent, as per Table 4.1.

Assumption 4.1.9. $f^{(1)}(W, v, \rho)$ is of class C^2 , is positive, has bounded derivative, and is strictly convex with respect to the airspeed v for $v > 0$. For climb and descent, $f^{(0)}(T, v, \rho)$ is of class C^2 , is positive, has bounded derivative, is linear in T and its derivative with respect to T is positive.

Table 4.1: Aircraft Dynamics Parameters in Climb and Descent

Engine Type	$f^{(0)}$, [J/s]	$f^{(1)}$, [J/s]	Fuel-Flow Coefficient, b
Turbojet	$eS_{FC}T$	$eS_{FC}D(W, v, \rho)$	$b = 0$
Turbofan	$eS_{FC}T$	$eS_{FC}D(W, v, \rho)$	$b > 0$
Turboprop	$eS_{FC}Tv$	$eS_{FC}D(W, v, \rho)v$	$b = 0$
All-Electric	$\frac{1}{\eta}Tv$	$\frac{1}{\eta}D(W, v, \rho)v$	N/A

4.2 Maximum Endurance OCP

In this section, the maximum endurance problem will be formulated over the climb, cruise, and descent phases of flight using the hybrid optimal control framework described in [17]. The discrete states of flight are defined in (144) and the energy and altitude dynamics are given by (146) and (145), respectively.

The performance index is defined as

$$J^* = \max \int_{t_c}^{t_d} dt \quad (147)$$

such that the endurance time in cruise is maximized.

The aircraft will switch to cruise once it reaches the desired cruising altitude, as defined by the switching manifold

$$\psi^{(1)} = h(t_c) - h_c = 0 \quad (148)$$

The aircraft will then switch to descent once it has a certain amount of stored energy remaining, as defined by the switching manifold

$$\psi^{(2)} = E(t_d) - E_d = 0 \quad (149)$$

From the dynamics in (146) and (145), and the performance index (147), the hybrid optimal control problem is

$$\begin{aligned}
J^* &= \max_{v, T, t_c, t_d, t_f} \int_{t_c}^{t_d} dt \\
&\text{s.t.} \\
\dot{x} &= v + \omega \\
\dot{h} &= \begin{cases} 0 & \text{for } t_c \leq t \leq t_d \\ \frac{v(T-D)}{W} & \text{otherwise} \end{cases} \\
\dot{E} &= \begin{cases} -f^{(1)}(W, v, \rho) & \text{for } t_c \leq t \leq t_d \\ -f^{(0)}(T, v, \rho) & \text{otherwise} \end{cases} \\
\psi^{(1)} &= h(t_c) - h_c = 0 \\
\psi^{(2)} &= E(t_d) - E_d = 0 \\
E(t_0) &= E_0, E(t_d) = E_d, E(t_f) = E_f \\
h(t_0) &= h_0, h(t) = h_c \text{ for } t_c \leq t \leq t_d \\
v &> 0 \\
T_{idle} &\leq T \leq T_{max}(h) \\
D &= \frac{1}{2}\rho S C_{D0} v^2 + \frac{2C_{D2} W^2}{\rho S v^2}
\end{aligned} \quad (150)$$

Remark 2. *The constraint that $v > 0$ ensures that the aircraft will only travel in one forward direction during flight. However, the true minimum airspeed is limited by the stall speed of the aircraft, as described in Section 2.1.3. In order to ensure feasibility of the solution, it should be verified that the resulting optimal airspeed for a particular aircraft is greater than its stall speed.*

4.3 Maximum Endurance Solution

This section provides a general solution to the maximum endurance problem (150).

Theorem 9. *The maximum endurance airspeed v^* is defined for each stage of flight as*

$$v^* = \begin{cases} v^{*(0)} \text{ is the solution of } \frac{f^{(0)}(T, v, \rho)}{v(T-D)}(T - D - vD_v) - f_v^{(0)}(T, v, \rho) = 0 & \text{for } t_0 \leq t < t_c \\ v^{*(1)} \text{ is the solution of } f_v^{(1)}(W, v, \rho) = 0 & \text{for } t_c \leq t \leq t_d \\ v^{*(2)} \text{ is the solution of } \frac{f^{(0)}(T, v, \rho)}{v(T-D)}(T - D - vD_v) - f_v^{(0)}(T, v, \rho) = 0 & \text{for } t_d < t \leq t_f \end{cases} \quad (151)$$

and the optimal thrust profile is

$$T^* = \begin{cases} T^{*(0)} = T_{max}(h) & \text{for } t_0 \leq t < t_c \\ T^{*(1)} = D(W, v^{*(1)}, \rho) & \text{for } t_c \leq t \leq t_d \\ T^{*(2)} = T_{idle} & \text{for } t_d < t \leq t_f \end{cases} \quad (152)$$

and the endurance time is

$$J^* = \int_{t_c}^{t_d} dt = - \int_{E_c}^{E_d} \frac{1}{f^{(1)}(W, v^{*(1)}, \rho)} dE \quad (153)$$

Proof. In climb, the Hamiltonian is defined as

$$H^{(0)} = -J_E^* f^{(0)}(T, v, \rho) + J_h^* \frac{v(T-D)}{W} + J_x^*(v + \omega) \quad \text{for } t_0 \leq t < t_c \quad (154)$$

and in cruise, the Hamiltonian is given by

$$H^{(1)} = 1 - J_E^* f^{(1)}(W, v, \rho) + J_x^*(v + \omega) \quad \text{for } t_c < t < t_d \quad (155)$$

Finally, in descent the Hamiltonian is

$$H^{(2)} = -J_E^* f^{(0)}(T, v, \rho) + J_h^* \frac{v(T-D)}{W} + J_x^*(v + \omega) \quad \text{for } t_d < t \leq t_f \quad (156)$$

At the switching instances t_c (climb to cruise) and t_d (cruise to descent), the following necessary

conditions must hold. At top of climb, the conditions are

$$\begin{aligned}
J_E^*(t_{c-}) &= J_E^*(t_{c+}) + \nu_E^{(1)} \left(\frac{\partial \psi^{(1)}}{\partial E(t_c)} \right) \\
J_h^*(t_{c-}) &= J_h^*(t_{c+}) + \nu_h^{(1)} \left(\frac{\partial \psi^{(1)}}{\partial h(t_c)} \right) \\
J_x^*(t_{c-}) &= J_x^*(t_{c+}) + \nu_x^{(1)} \left(\frac{\partial \psi^{(1)}}{\partial x(t_c)} \right)
\end{aligned} \tag{157}$$

and at top of descent, the conditions are

$$\begin{aligned}
J_E^*(t_{d-}) &= J_E^*(t_{d+}) + \nu_E^{(2)} \left(\frac{\partial \psi^{(2)}}{\partial E(t_d)} \right) \\
J_h^*(t_{d-}) &= J_h^*(t_{d+}) + \nu_h^{(2)} \left(\frac{\partial \psi^{(2)}}{\partial h(t_d)} \right) \\
J_x^*(t_{d-}) &= J_x^*(t_{d+}) + \nu_x^{(2)} \left(\frac{\partial \psi^{(2)}}{\partial x(t_d)} \right)
\end{aligned} \tag{158}$$

where $\nu_E^{(1)}$, $\nu_h^{(1)}$, $\nu_x^{(1)}$, $\nu_E^{(2)}$, $\nu_h^{(2)}$, and $\nu_x^{(2)}$ are scalars. Evaluating the partial derivatives in (157) and (158) yields

$$\frac{\partial \psi^{(1)}}{\partial E(t_c)} = 0, \quad \frac{\partial \psi^{(1)}}{\partial h(t_c)} = 1, \quad \frac{\partial \psi^{(1)}}{\partial x(t_c)} = 0, \quad \frac{\partial \psi^{(2)}}{\partial E(t_d)} = 1, \quad \frac{\partial \psi^{(2)}}{\partial h(t_d)} = 0, \quad \frac{\partial \psi^{(2)}}{\partial x(t_d)} = 0 \tag{159}$$

Therefore, at the switching times t_c and t_d , the following relations must hold for the costates

$$\begin{aligned}
J_E^*(t_{c-}) &= J_E^*(t_{c+}) \\
J_h^*(t_{c-}) &= J_h^*(t_{c+}) + \nu_h^{(1)} \\
J_x^*(t_{c-}) &= J_x^*(t_{c+})
\end{aligned} \tag{160}$$

$$\begin{aligned}
J_E^*(t_{d-}) &= J_E^*(t_{d+}) + \nu_E^{(2)} \\
J_h^*(t_{d-}) &= J_h^*(t_{d+}) \\
J_x^*(t_{d-}) &= J_x^*(t_{d+})
\end{aligned} \tag{161}$$

From (160), there is a jump discontinuity in J_h^* at t_c if $\nu_h^{(1)} \neq 0$ and J_E^* is continuous at t_c . Similarly, from (161), there is a jump discontinuity in J_E^* at t_d if $\nu_E^{(2)} \neq 0$, but J_h^* is continuous at t_c . The costate J_x^* experiences no jump discontinuities.

The dynamics in the costate J_x^* are defined by Hamilton's equations as

$$\dot{J}_x^* = \begin{cases} -\frac{\partial H^{(0)}}{\partial x} & \text{for } t_0 \leq t < t_c \\ -\frac{\partial H^{(1)}}{\partial x} & \text{for } t_c < t < t_d \\ -\frac{\partial H^{(2)}}{\partial x} & \text{for } t_d < t \leq t_f \end{cases} \quad (162)$$

Since the Hamiltonian does not depend on x in any stage of flight (154), (155), (156), the costate J_x^* will be constant since

$$\dot{J}_x^* = 0 \quad \text{for } t_0 \leq t \leq t_f \quad (163)$$

Furthermore, since the final position is free, $J_x^*(t_f) = 0$. From free final position and the continuity conditions (160) and (161), J_x^* will be identically zero

$$J_x^*(t) = 0 \quad \text{for } t_0 \leq t \leq t_f \quad (164)$$

Therefore, the Hamiltonians in climb, cruise and descent are simplified to

$$H^{(0)} = -J_E^* f^{(0)}(T, v, \rho) + J_h^* \frac{v(T-D)}{W} \quad \text{for } t_0 \leq t < t_c \quad (165a)$$

$$H^{(1)} = 1 - J_E^* f^{(1)}(W, v, \rho) \quad \text{for } t_c < t < t_d \quad (165b)$$

$$H^{(2)} = -J_E^* f^{(0)}(T, v, \rho) + J_h^* \frac{v(T-D)}{W} \quad \text{for } t_d < t \leq t_f \quad (165c)$$

Next, the necessary conditions in the Hamiltonians at times t_c and t_d are

$$\begin{aligned} H^{(0)}(t_{c-}) &= H^{(1)}(t_{c+}) - \nu_H^{(1)} \frac{\partial \psi^{(1)}}{\partial t_c} \\ H^{(1)}(t_{d-}) &= H^{(2)}(t_{d+}) - \nu_H^{(2)} \frac{\partial \psi^{(2)}}{\partial t_d} \end{aligned} \quad (166)$$

where $\nu_H^{(1)}$ and $\nu_H^{(2)}$ are constant scalars, and the partial derivative in (166) are

$$\frac{\partial \psi^{(1)}}{\partial t_c} = 0, \quad \frac{\partial \psi^{(2)}}{\partial t_d} = 0 \quad (167)$$

which implies that

$$H^{(0)}(t_{c-}) = H^{(1)}(t_{c+}) \quad (168)$$

and

$$H^{(1)}(t_{d-}) = H^{(2)}(t_{d+}) \quad (169)$$

In other words, from (168) and (169), the Hamiltonian is continuous. Moreover, since the Hamiltonian does not explicitly depend on time and final time is free, then

$$H^{(1)} = H^{(2)} = H^{(3)} = 0 \quad (170)$$

The rest of the proof will be broken down into four sections: the cruise, the climb, the descent phases of flight, and the computation of the endurance.

I. Cruise

First, it will be shown that J_E^* is positive in cruise, as this will be necessary in determining the optimal airspeed profile. In cruise, the Hamiltonian is (165b). From (170), the costate J_E^* is

$$J_E^* = \frac{1}{f^{(1)}(W, v, \rho)}, \quad t_c < t < t_d \quad (171)$$

Since $f^{(1)}$ is positive from Assumption 4.1.9, the costate J_E^* is also positive in cruise. The necessary condition in v is

$$H_v^{(1)} = -J_E^* f_v^{(1)}(W, v, \rho) = 0 \quad (172)$$

Since from (171) $J_E^* > 0$, the necessary condition (172) is equivalent to

$$f_v^{(1)}(W, v, \rho) = 0 \quad (173)$$

Therefore, the optimal airspeed profile in cruise can be found by solving for $v^{*(1)}$ in the necessary condition $f_v^{(1)}(W, v^{*(1)}, \rho) = 0$.

From Assumption 4.1.4, the optimal thrust profile is

$$T^{*(1)} = D(W, v^{*(1)}, \rho) \quad (174)$$

II. Climb

First, it will be shown that the costate J_E^* is positive in climb. This will be necessary to determine the optimal airspeed and thrust profiles later. In climb, the Hamiltonian is (165a). From (170), the costates J_h^* and J_E^* can be related by

$$J_h^* = J_E^* \frac{f^{(0)}(T, v, \rho) W}{v(T - D)}, \quad t_0 \leq t < t_c \quad (175)$$

Note that $T > D$ in climb from equation (142) with $W > 0$ and $\gamma > 0$.

Furthermore, from (160) and (171), at top of climb, the costate J_E^* is given by

$$J_E^*(t_{c-}) = J_E^*(t_{c+}) = \frac{1}{f^{(1)}(W, v, \rho)} \Big|_{t=t_{c+}} > 0 \quad (176)$$

The dynamics of the costate J_E^* in climb are

$$\dot{J}_E^* = -\frac{\partial H^{(0)}}{\partial E} \quad \text{for } t < t_c \quad (177)$$

which is equivalent to

$$\dot{J}_E^* = -\frac{\partial H^{(0)}}{\partial W} \frac{dW}{dE} \quad \text{for } t < t_c \quad (178)$$

From the energy model in Section 2.1.7, the conversion from weight to energy for fuel-burning aircraft is

$$E = eW_{fuel} = e(W - W_f) \quad (179)$$

where the fuel available is $W - W_f$. Isolating for W yields

$$W = \frac{E}{e} + W_f \quad (180)$$

Therefore, W_E is

$$W_E = \frac{dW}{dE} = \frac{1}{e} > 0 \quad \text{for fuel-burning aircraft} \quad (181)$$

and is a constant. In the case of the all-electric aircraft, there is no fuel weight since the energy comes from the battery, so the derivative is

$$W_E = 0 \quad \text{for all-electric aircraft} \quad (182)$$

Therefore for all aircraft, we have

$$\frac{dW}{dE} \geq 0 \quad (183)$$

Next, the first partial derivative in (178) is

$$\frac{\partial H^{(0)}}{\partial W} = -J_h^* v \left(\frac{T - D}{W^2} + \frac{D_W}{W} \right) \quad (184)$$

replacing (175) into (184) yields

$$\frac{\partial H^{(0)}}{\partial W} = -J_E^* f^{(0)}(T, v, \rho) \left(\frac{1}{W} + \frac{D_W}{T - D} \right) \quad (185)$$

Replacing (185) into (178) yields

$$J_E^* = J_E^* f^{(0)}(T, v, \rho) \left(\frac{1}{W} + \frac{D_W}{T - D} \right) \frac{dW}{dE} \quad (186)$$

The differential equation (186) is separable and can be integrated as

$$\int \frac{1}{J_E^*} dJ_E^* = \int \left(f^{(0)}(T, v, \rho) \left(\frac{1}{W} + \frac{D_W}{T-D} \right) \frac{dW}{dE} \right) dt + k_1 \quad (187)$$

Solving the left hand side of (187) yields

$$\ln(J_E^*) - k_1 = \int \left(f^{(0)}(T, v, \rho) \left(\frac{1}{W} + \frac{D_W}{T-D} \right) \frac{dW}{dE} \right) dt \quad (188)$$

where k_1 is a constant of integration. Isolating for J_E^* yields

$$J_E^* = k_2 e^{\int \left(f^{(0)}(T, v, \rho) \left(\frac{1}{W} + \frac{D_W}{T-D} \right) \frac{dW}{dE} \right) dt} \quad (189)$$

where $k_2 = e^{k_1}$ and is a positive constant. The costate J_E^* is therefore positive.

Next, the optimal airspeed profile will be derived. From (165a), the necessary condition in v during climb is

$$H_v^{(0)} = -J_E^* f_v^{(0)} + \frac{J_h^*}{W} (T - D - vD_v) = 0 \quad (190)$$

Replacing (175) into (190) yields

$$H_v^{(0)} = -J_E^* f_v^{(0)} + J_E^* \frac{f_h^{(0)}(T, v, \rho)}{v(T-D)} (T - D - vD_v) = 0 \quad (191)$$

which can be rearranged as

$$H_v^{(0)} = J_E^{*(0)} \left(\frac{f_h^{(0)}(T, v, \rho)}{v(T-D)} (T - D - vD_v) - f_v^{(0)} \right) = 0 \quad (192)$$

Since from (189) $J_E^* > 0$ and from equation (142) $T > D$, the necessary condition is equivalent to

$$\frac{f_h^{(0)}(T, v, \rho)}{v(T-D)} (T - D - vD_v) - f_v^{(0)} = 0 \quad (193)$$

Finally, the optimal thrust profile in climb will be derived. From Assumption 4.1.9

$$f^{(0)}(T, v, \rho) = f_T^{(0)}(v, \rho) T \quad (194)$$

Replacing (194) into (165a) and isolating for T yields

$$H^{(0)} = \left(J_h^* \frac{v}{W} - J_E^* f_T^{(0)}(v, \rho) \right) T - J_h^* \frac{vD}{W} \quad (195)$$

Substituting J_h^* by (175) in the first term yields

$$H^{(0)} = \left(\frac{J_E^*}{T-D} f_T^{(0)} D \right) T - J_h^* \frac{vD}{W} \quad (196)$$

(the arguments for $f_T^{(0)}$ were omitted for simplicity). Defining a switching function ζ as

$$\zeta = \frac{J_E^*}{T-D} f_T^{(0)} D \quad (197)$$

Then the optimal thrust will be obtained according to

$$\max_T \left\{ H^{(0)} \right\} = \max_T \left\{ \zeta T - J_h^* \frac{vD}{W} \right\} \quad (198)$$

Since T is bounded according to Assumption 4.1.8, the optimal thrust profile will depend on the sign of ζ . If ζ is positive, the optimal thrust profile will be $T_{max}(h)$, and if ζ is negative it will be T_{idle} . Since J_E^* is strictly positive from (189), $f_T^{(0)}$ is strictly positive from Assumption 4.1.9, and D is strictly positive from (81), ζ will never be zero. The sign of ζ will depend on the $T - D$ term where

$$\zeta > 0 \text{ for } T > D \quad (199)$$

$$\zeta < 0 \text{ for } T < D$$

Therefore in climb when $T > D$, ζ will be positive. Since ζ is positive for climb, the optimal thrust in climb is

$$T^{*(0)} = T_{max}(h) \quad (200)$$

III. Descent

The descent portion of flight closely resembles the climb portion of flight since the Hamiltonians are identical. First, it will be shown that the costate J_E^* is positive during descent as this will again be necessary in determining the optimal airspeed and thrust profiles later. The costate dynamics \dot{J}_E^* in descent are identical to those in climb (186) since in descent, the Hamiltonian (165c) is identical to the Hamiltonian in climb (165a). Moreover, it follows that J_E^* is equal to

$$J_E^* = k_2 e^{\int \left(f^{(0)} \left(\frac{1}{W} + \frac{D}{T-D} \right) \frac{\partial W}{\partial E} \right) dt} \quad (201)$$

where $k_2 = e^{-k_1}$ and is a positive constant. The costate J_E^* is therefore positive during descent.

Since the Hamiltonian in descent (165c) is identical to the Hamiltonian in climb (165a), the necessary condition in v is identical to (193). The first derivative of the Hamiltonian with respect to v is

$$H_v^{(2)} = J_E^* \left(\frac{f^{(2)}}{v(T-D)} (T - D - vD_v) - f_v^{(2)} \right) = 0 \quad (202)$$

From (201) $J_E^* > 0$, therefore (202) is equivalent to the following necessary condition in v

$$\frac{f^{(2)}}{v(T-D)} (T - D - vD_v) - f_v^{(2)} = 0 \quad (203)$$

Finally, the optimal thrust profile in descent will be derived. Similarly to (198)

$$\max_T \left\{ H^{(2)} \right\} = \max_T \left\{ \zeta T - J_h^* \frac{vD}{W} \right\} \quad (204)$$

where ζ is given by (197). From Assumption 4.1.3 $T < D$ in descent, therefore ζ will be negative.

The optimal thrust in descent is therefore the minimum allowable thrust

$$T^{*(2)} = T_{idle} \quad (205)$$

IV. Endurance

The maximum endurance can be found by solving the differential equation

$$\dot{E} = \frac{dE}{dt} = -f^{(1)}(W, v^{*(1)}, \rho) \quad (206)$$

from top of climb to top of descent and evaluated at $v = v^{*(1)}$. From Assumption 4.1.9 $f^{(1)} > 0$.

The total endurance is therefore

$$J^* = \int_{t_c}^{t_d} dt = - \int_{E_c}^{E_d} \frac{1}{f^{(1)}(W, v^{*(1)}, \rho)} dE \quad (207)$$

□

Remark 3. *The expression for maximum endurance (207) depends on E_c and E_d . The energy at top of descent E_d is known and the energy at top of climb E_c can be related to the cruising altitude h_c through the set of differential equations for climb given by*

$$\begin{aligned} \frac{dE}{dt} &= -f^{(0)}(T^{*(0)}, v^{*(0)}) \\ \frac{dh}{dt} &= \frac{v^{*(0)}(T^{*(0)} - D)}{W} \end{aligned} \quad (208)$$

which can be rearranged as

$$\frac{dE}{dh} = - \frac{f^{(0)}(T^{*(0)}, v^{*(0)}) W}{v^{*(0)}(T^{*(0)} - D)} \quad (209)$$

where $T > D$ in climb from Assumption 4.1.3. In general, (209) is not separable and therefore analytical solutions are difficult to find. However, it can be integrated numerically with initial conditions $E(t_0) = E_0$ and $h(t_0) = h_0$ and final altitude $h(t_c) = h_c$ to solve for the energy at top of climb $E(t_c) = E_c$. The energy at top of climb E_c can then be replaced into the integral (207) to solve for the endurance time.

4.4 Solved Examples

The results of Section 4.3 can be applied to specific engine configurations using the energy-depletion dynamics given for each aircraft in Table 4.1. The optimal thrust profile is identical for all aircraft, and is given by (152). This section provides the optimal airspeed profile for climb, cruise, and descent for each aircraft. A summary of the results is given in Table 4.2 in Section 4.6.

4.4.1 Turbojet

The maximum endurance problem (150) can be solved for a turbojet following the procedure of Section 4.3. From the results of Theorem 9, the optimal thrust profile is given by (152).

Replacing the dynamics for a turbojet in climb and the optimal thrust curve into the necessary condition in v for climb (193) yields

$$\frac{-S_{FC}T_{max}}{v(T_{max} - D)}(T_{max} - D - vD_v) = 0 \quad (210)$$

Since S_{FC} , T_{max} , and v are strictly positive, and $T_{max} > D$, the necessary condition is equivalent to

$$T_{max} - D - vD_v = 0 \quad (211)$$

Substituting (81) for drag yields

$$T_{max} - \frac{1}{2}\rho SC_{D0}v^2 - \frac{2C_{D2}W^2}{\rho Sv^2} - \rho SC_{D0}v^2 + \frac{4C_{D2}W^2}{\rho Sv^2} = 0 \quad (212)$$

Rearranging the terms gives

$$T_{max} - \frac{3}{2}\rho SC_{D0}v^2 + \frac{2C_{D2}W^2}{\rho Sv^2} = 0 \quad (213)$$

which can be rewritten as the following bi-quadratic in v

$$\frac{3}{2}\rho SC_{D0}v^4 - T_{max}v^2 - \frac{2C_{D2}W^2}{\rho S} = 0 \quad (214)$$

Solving for v yields only one real, positive solution, which is

$$v^2 = \frac{T_{max} + \sqrt{T_{max}^2 + 12W^2C_{D0}C_{D2}}}{3\rho SC_{D0}} \quad (215)$$

and corresponds to the maximum rate of climb [27]. The optimal airspeed profile in climb is therefore

$$v^{*(0)} = \sqrt{\frac{T_{max} + \sqrt{T_{max}^2 + 12W^2C_{D0}C_{D2}}}{3\rho SC_{D0}}} \quad (216)$$

In descent, the necessary condition in v is identical to that in climb. Therefore, the same procedure can be applied as in (210) to (215) with the only difference being that the optimal thrust in descent is the idle thrust. Therefore, the optimal airspeed profile in descent is

$$v^{*(2)} = \sqrt{\frac{T_{idle} + \sqrt{T_{idle}^2 + 12W^2C_{D0}C_{D2}}}{3\rho SC_{D0}}} \quad (217)$$

which similarly corresponds to the minimum rate of descent [27].

The solution for the cruise portion of flight is provided in Section 3.4.1 and the optimal airspeed profile is (101).

4.4.2 Turbofan

The maximum endurance problem (150) can be solved for a turbofan following the procedure of Section 4.3. From the results of Theorem 9, the optimal thrust profile is given by (152).

Replacing the dynamics for a turbofan in climb and the optimal thrust curve into the necessary condition in v for climb (193) yields

$$\frac{a(1 + \frac{bv}{c})T}{v(T - D)}(T - D - vD_v) + \frac{ab}{c}T = 0 \quad (218)$$

Multiplying both sides by $v(T - D)/Ta$ yields

$$T - D - vD_v + \frac{bv}{c}(T - D) - \frac{bv}{c}vD_v - \frac{bv}{c}(T - D) = 0 \quad (219)$$

which simplifies to

$$T - D - vD_v + \left(1 + \frac{bv}{c}\right)vD_v = 0 \quad (220)$$

Expanding the drag terms and it's derivative gives

$$T - \frac{3}{2}\rho SC_{D0}v^2 + \frac{2C_{D2}W^2}{\rho Sv^2} - \frac{b}{c}\rho SC_{D0}v^3 + \frac{b}{c}\frac{4C_{D2}W^2}{\rho Sv} = 0 \quad (221)$$

Multiplying by v^2 yields the following 5th order polynomial in v

$$\frac{b}{c}\rho SC_{D0}v^5 + \frac{3}{2}\rho SC_{D0}v^4 - Tv^2 - \frac{b}{c}\frac{4C_{D2}W^2}{\rho S}v - \frac{2C_{D2}W^2}{\rho S} = 0 \quad (222)$$

From Descartes rule of signs, (222) will have one real zero. The zero of (222) corresponds to the optimal airspeed profile in climb for $T = T_{max}(h)$ and the optimal airspeed profile in descent when $T = T_{idle}$. Since there is no analytical expression for finding the zeros of a quintic polynomial of the form in (222), numerical solutions will be provided.

The solution for the cruise portion of flight also requires finding the root of a 5th order polynomial (105). However, in Section 3.4.2 an approximate analytical solution is provided and is given by (112).

4.4.3 Turboprop

The maximum endurance problem (150) can be solved for a turboprop following the procedure of Section 4.3. From the results of Theorem 9, the optimal thrust profile is given by (152).

Replacing the dynamics for a turboprop in climb and the optimal thrust curve into the necessary condition in v for climb (193) yields

$$\frac{S_{FC}Tv}{v(T-D)}(T - D - vD_v) - S_{FC}T = 0 \quad (223)$$

which is equivalent to

$$S_{FC}T(T - D - vD_v) - S_{FC}T(T - D) = 0 \quad (224)$$

Dividing the equation by $S_{FC}T$ and simplifying gives

$$vD_v = 0 \quad (225)$$

Expanding (225) and multiplying by v yields the following bi-quadratic equation in v

$$\rho S C_{D0} v^2 - \frac{4C_{D2}W^2}{\rho S v^2} = 0 \quad (226)$$

The optimal airspeed is the solution to (226). Since the necessary condition is identical in climb and cruise, and since (226) does not depend on T , the optimal airspeed profile will be the same in climb and descent, and is given by

$$v^{*(0)} = v^{*(2)} = \sqrt{\frac{2W}{\rho S} \sqrt{\frac{C_{D2}}{C_{D0}}}} \quad (227)$$

The solution for the cruise portion of flight is provided in Section 3.4.3 and the optimal airspeed profile is (130).

4.4.4 All-Electric

The maximum endurance problem (150) can be solved for an all-electric aircraft following the procedure of Section 4.3. From the results of Theorem 9, the optimal thrust profile is given by (152).

Replacing the dynamics for an all-electric aircraft in climb and the optimal thrust curve into the necessary condition in v for climb (193) yields

$$\frac{Tv}{v(T-D)}(T-D-vD_v) - T = 0 \quad (228)$$

which for $T \neq D$ reduces to

$$vD_v = 0 \quad (229)$$

Expanding (229) and multiplying by v yields to following bi-quadratic equation in v

$$\rho S C_{D0} v^2 - \frac{4 C_{D2} W^2}{\rho S v^2} = 0 \quad (230)$$

The optimal airspeed is the solution to (230). Since the necessary condition is identical in climb and cruise, and since (230) does not depend on T , the optimal airspeed profile will be the same in climb and descent, and is given by

$$v^{*(0)} = v^{*(2)} = \sqrt{\frac{2W}{\rho S}} \sqrt{\frac{C_{D2}}{C_{D0}}} \quad (231)$$

The solution for the cruise portion of flight is provided in Section 3.4.4 and the optimal airspeed profile is (136).

4.5 Aircraft Configurations

4.5.1 Aircraft Parameters

A table of the aircraft parameters for each example is provided in Table 3.2 of Section 3.5.1.

4.5.2 Turbojet

The cruise portion of the flight was already simulated in Section 3.5. The climb portion was simulated using a desired cruising altitude of 11,000 m. Flying at the optimal airspeed and thrust profiles for climb, the total endurance time in cruise was 14.09 hours. Figure 4.2 shows the optimal airspeed and thrust profiles in climb. Figure 4.3 shows the weight and altitude trajectories.

In order to validate that the optimal thrust in climb is maximum thrust, a comparison was made for different thrust profiles. Since maximum thrust depends on altitude, the maximum thrust profile was multiplied by a constant k to scale down the thrust profile with values of k between 0.55 and 0.95. Figure 4.4 illustrates the effect of a decreased thrust profile on the time to reach the desired cruising altitude. At values for k below 0.55, the aircraft ran out of fuel before reaching the desired cruising altitude and as a result had no endurance time in cruise.

Figure 4.5 shows the effect of the scaled down thrust profile on total cruise endurance. As expected, for values of k below 0.55, the aircraft will climb so slowly that there will not be sufficient

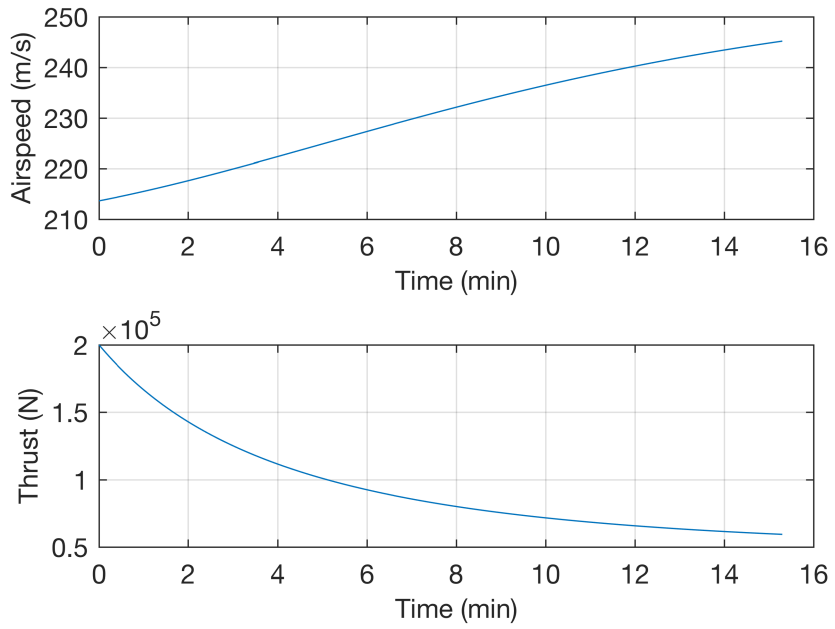


Figure 4.2: Optimal Airspeed and Thrust Profiles

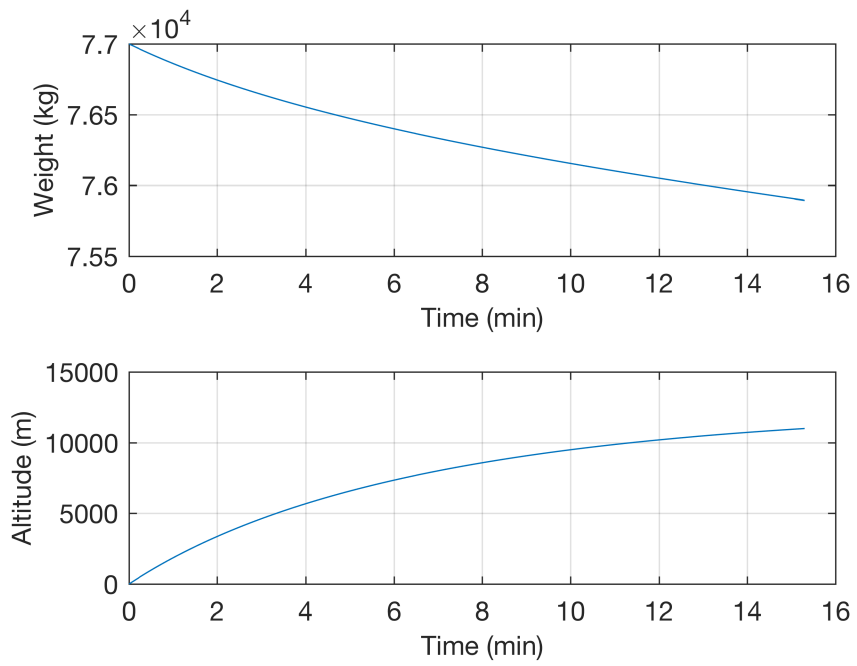


Figure 4.3: Weight and Altitude Trajectories

fuel to reach the desired altitude and the endurance time in cruise will be zero. However, it also shows that it is possible to decrease the thrust profile by up to 15% without significant losses in the cruise endurance.

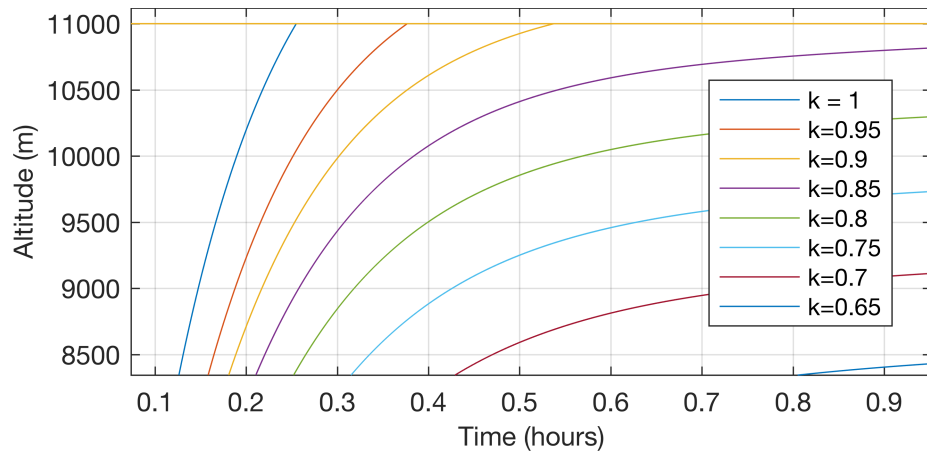


Figure 4.4: Altitude Profiles for Scaled Thrust Input

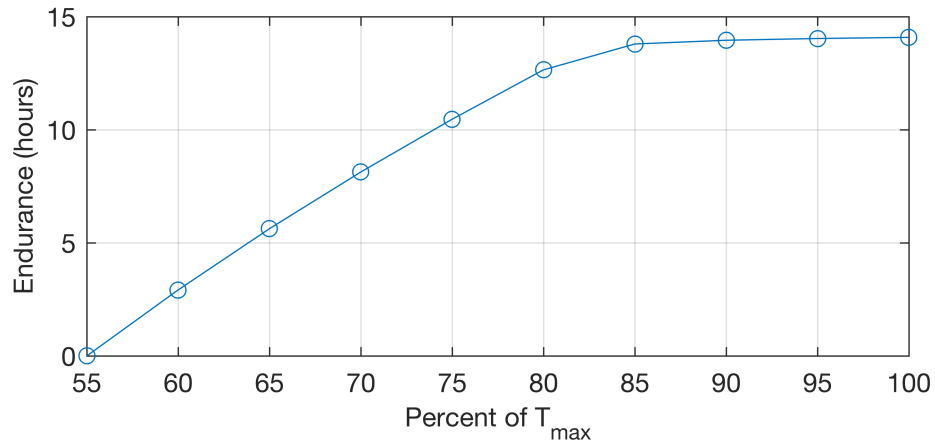


Figure 4.5: Effect of Reduced Thrust Profile on Endurance

4.5.3 Turbofan

The cruise portion of the flight was already simulated in Section 3.5. The climb portion was simulated using a desired cruising altitude of 11,000 m. Figure 4.6 shows the optimal airspeed and thrust profiles in climb. Figure 4.7 shows the weight and altitude trajectories.

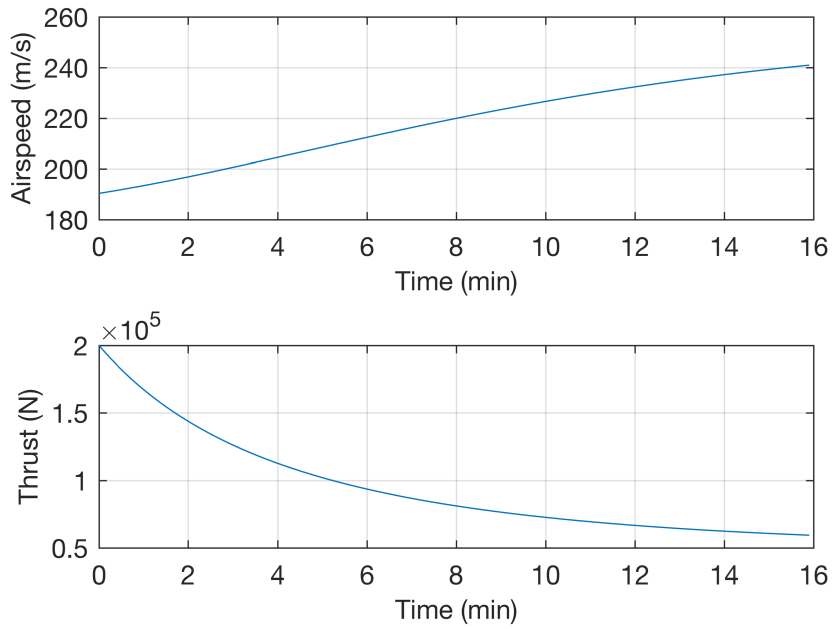


Figure 4.6: Optimal Airspeed and Thrust Profiles

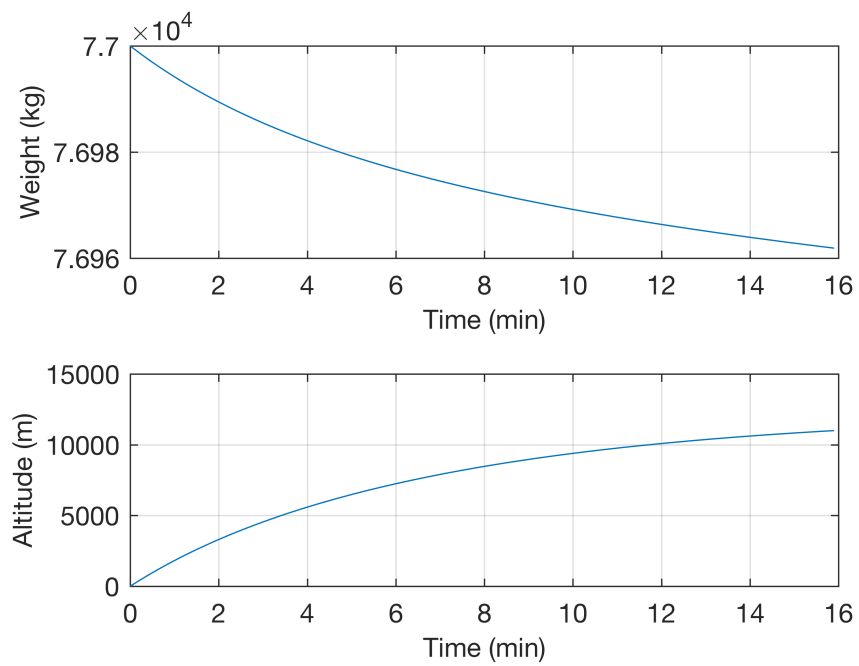


Figure 4.7: Weight and Altitude Trajectories

In order to validate that the optimal thrust in climb is maximum thrust, a comparison was made for different thrust profiles. Since maximum thrust depends on altitude, the maximum thrust profile was multiplied by a constant k to scale down the thrust profile with values of k between 0.55 and 0.95. Figure 4.8 illustrates the effect of a decreased thrust profile on the time to reach the desired cruising altitude. Going from left to right, the curves show decreasing values of k . At values for k below 0.55, the aircraft ran out of fuel before reaching the desired cruising altitude.

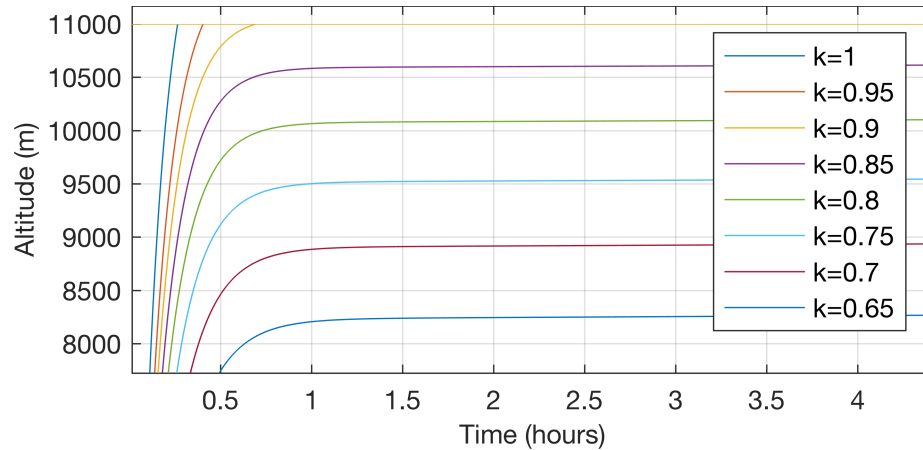
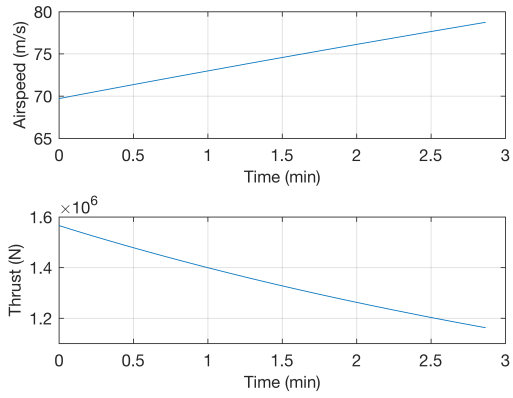


Figure 4.8: Altitude Profiles for Scaled Thrust Input

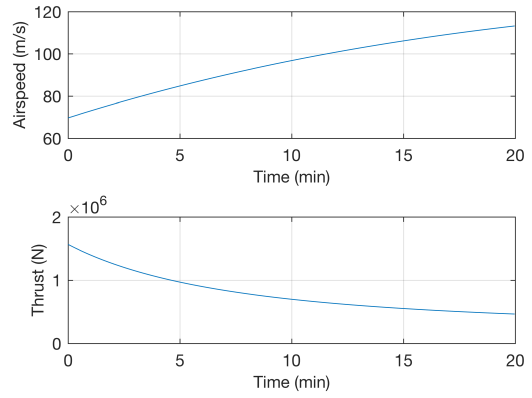
4.5.4 Turboprop

The cruise portion of the flight was already simulated in Section 3.5. Since the turboprop endurance is very sensitive to cruising altitude, two cruising altitudes were simulated: 3,000 m and 11,000 m. Flying at the optimal airspeed and thrust profiles for climb, the total endurance time in cruise was 7.33 hours for a cruising altitude of 3,000 m and 2.28 hours for a desired cruising altitude of 11,000 m. As expected, the higher cruising altitude caused a large reduction in endurance time for two reasons: because the turboprop is more efficient at lower altitudes and also because more fuel was burned during climb to reach the higher altitude. Figure 4.9 shows the optimal airspeed and thrust profiles in climb and Figure 4.10 shows the weight and altitude trajectories.

In order to validate that the optimal thrust in climb is maximum thrust, a comparison was made for different thrust profiles. Since maximum thrust depends on altitude, the maximum thrust profile was multiplied by a constant k to scale down the thrust profile. For a cruising altitude of 3,000 m,

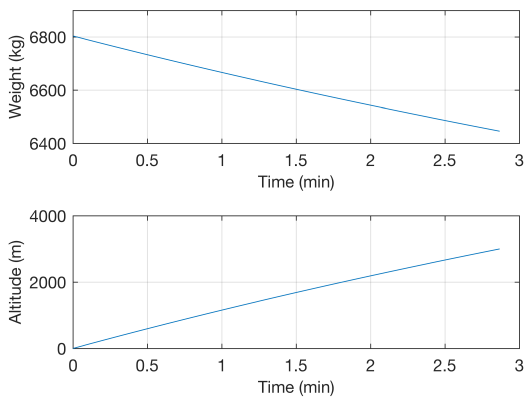


(a) Cruising Altitude of 3,000 m

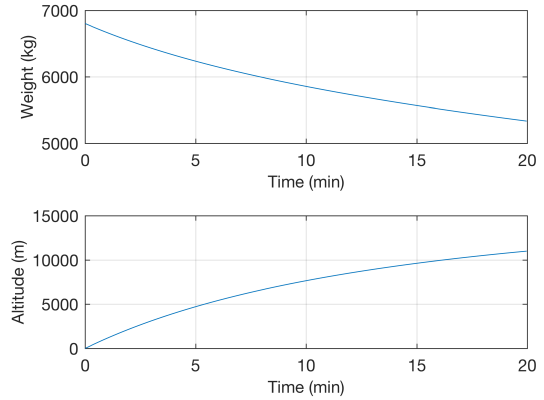


(b) Cruising Altitude of 11,000 m

Figure 4.9: Optimal Airspeed and Thrust Profiles



(a) Cruising Altitude of 3,000 m



(b) Cruising Altitude of 11,000 m

Figure 4.10: Weight and Altitude Trajectories

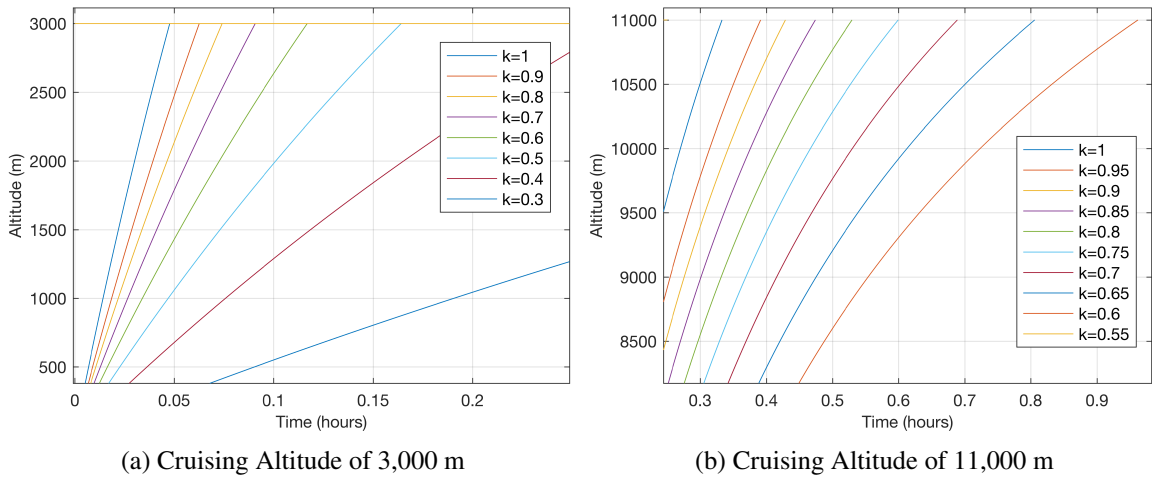


Figure 4.11: Altitude Profiles for Scaled Thrust Input

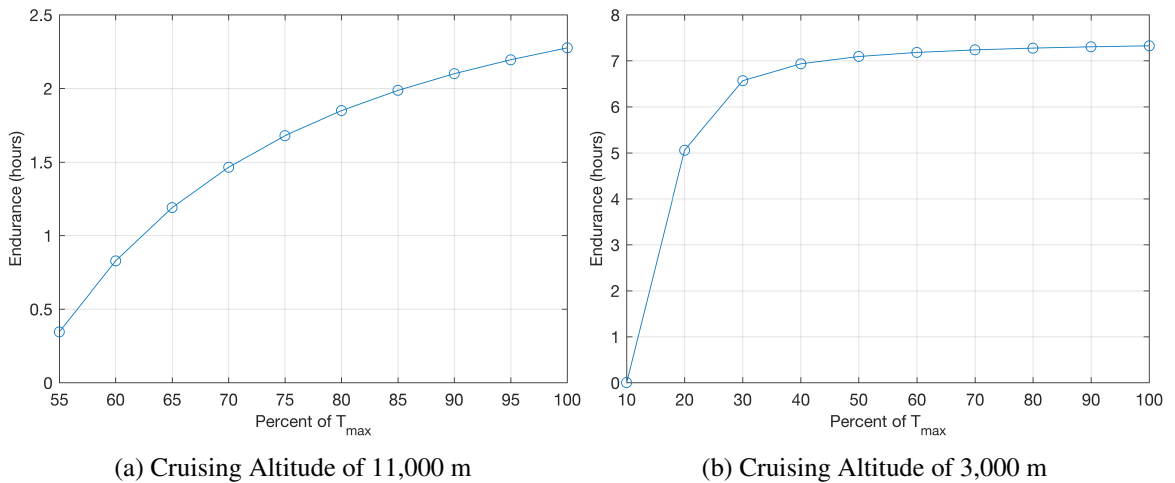


Figure 4.12: Effect of Reduced Thrust Profile on Endurance

values of k between 0.1 and 0.9 were used, and for 11,000 m values between 0.55 and 0.95 were used. Figure 4.11 illustrates the effect of a decreased thrust profile on the time to reach the desired cruising altitude.

Figure 4.12 shows the effect of the scaled down thrust profile on total cruise endurance. For a higher cruising altitude, the thrust effect was more significant than for a lower cruising altitude. For a cruising altitude of 3,000 m, the effect of scaling down the thrust was relatively small for a decrease of up to 50% of maximum thrust.

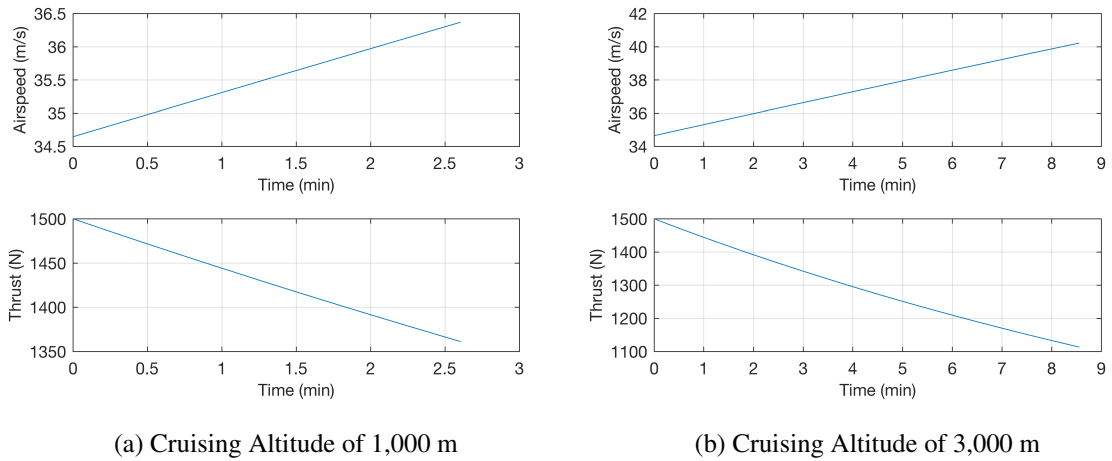


Figure 4.13: Optimal Airspeed and Thrust Profiles

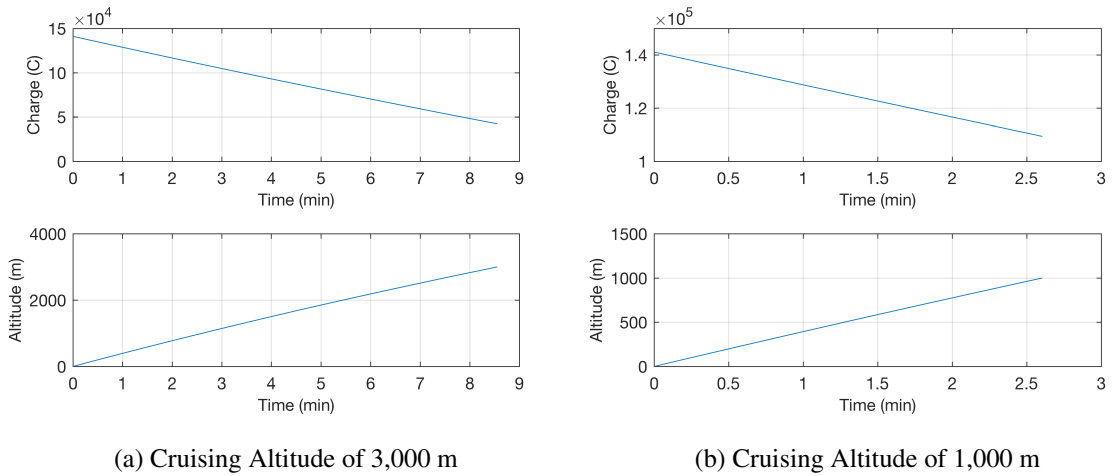


Figure 4.14: Weight and Altitude Trajectories

4.5.5 All-Electric

The cruise portion of the flight was already simulated in Section 3.5. Since the all-electric's cruise endurance is very sensitive to altitude, two cruising altitudes were simulated: 1,000 m and 3,000 m. Flying at the optimal airspeed and thrust profiles for climb, the total endurance time in cruise was around 48.5 minutes for a cruising altitude of 1,000 m, and around 17 minutes for a cruising altitude of 3,000 m. Figure 4.13 shows the optimal airspeed and thrust profiles in climb. Figure 4.10 shows the weight and altitude trajectories.

In order to validate that the optimal thrust in climb is maximum thrust, a comparison was made

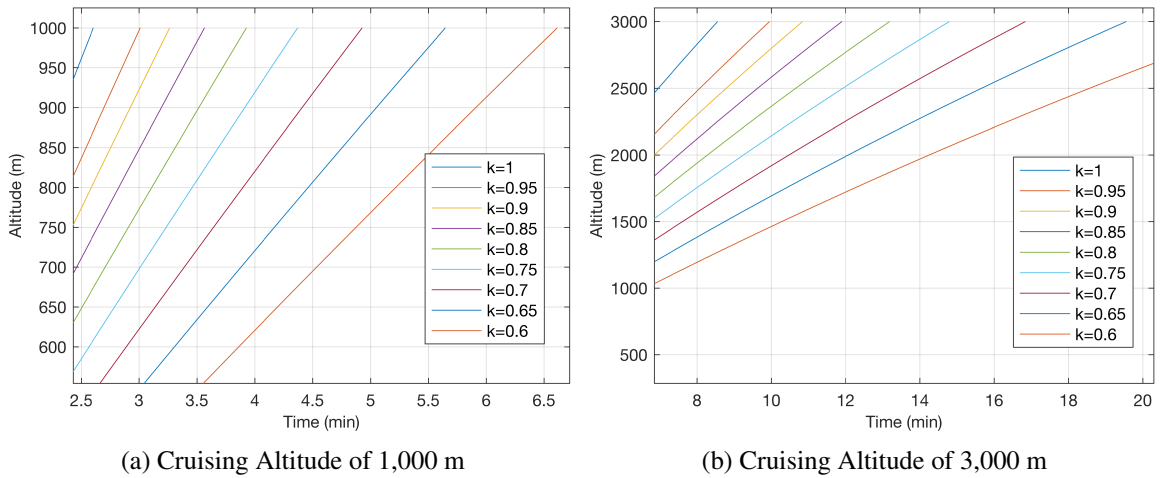


Figure 4.15: Altitude Profiles for Scaled Thrust Input

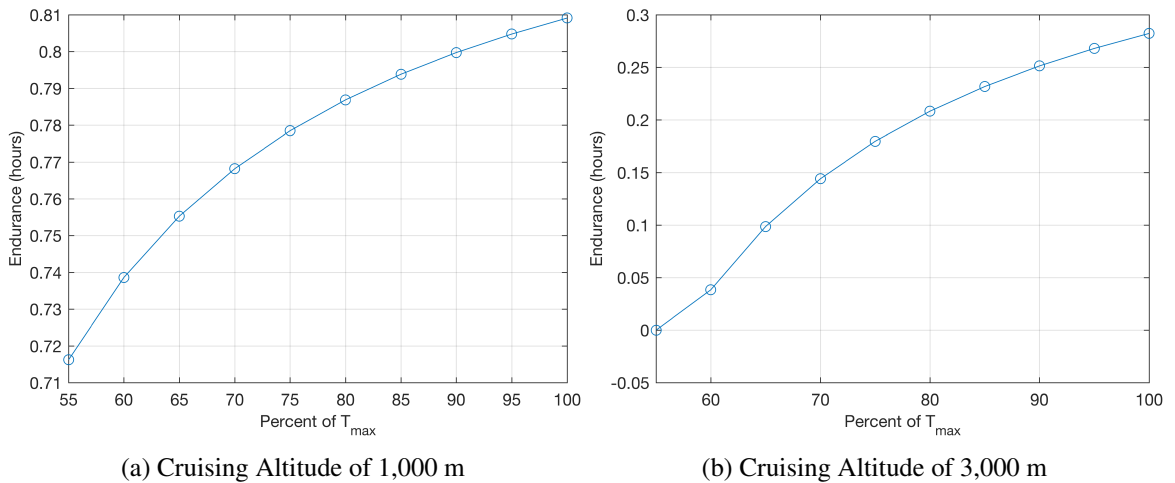


Figure 4.16: Effect of Reduced Thrust Profile on Endurance

for different thrust profiles. Since maximum thrust depends on altitude, the maximum thrust profile was multiplied by a constant k to scale down the thrust profile with values of k between 0.6 and 0.95. Figure 4.15 illustrates the effect of a decreased thrust profile on the time to reach the desired cruising altitude.

Figure 4.16 shows the effect of the scaled down thrust profile on total cruise endurance. The all-electric aircraft is very sensitive to altitude and even small reductions in climbing thrust reduce the available cruise endurance significantly.

4.6 Summary

A summary of the optimal airspeed profiles for climb, cruise, and descent is given in Table 4.2.

Table 4.2: Optimal Airspeed Profiles for Different Aircraft

Engine Type	Climb Airspeed Profile	Cruise Airspeed Profile	Descent Airspeed Profile
Turbojet	$\sqrt{\frac{T_{max} + \sqrt{T_{max}^2 + 12W^2 C_{D0} C_{D2}}}{3\rho S C_{D0}}}$	$\sqrt{\frac{2W}{\rho S}} \sqrt{\frac{C_{D2}}{C_{D0}}}$	$\sqrt{\frac{T_{idle} + \sqrt{T_{idle}^2 + 12W^2 C_{D0} C_{D2}}}{3\rho S C_{D0}}}$
Turbofan	No analytic solution	No analytic solution ¹	No analytic solution
Turboprop	$\sqrt{\frac{2W}{\rho S}} \sqrt{\frac{C_{D2}}{C_{D0}}}$	$\sqrt{\frac{2W}{\rho S}} \sqrt{\frac{C_{D2}}{3C_{D0}}}$	$\sqrt{\frac{2W}{\rho S}} \sqrt{\frac{C_{D2}}{C_{D0}}}$
All-Electric	$\sqrt{\frac{2W}{\rho S}} \sqrt{\frac{C_{D2}}{C_{D0}}}$	$\sqrt{\frac{2W}{\rho S}} \sqrt{\frac{C_{D2}}{3C_{D0}}}$	$\sqrt{\frac{2W}{\rho S}} \sqrt{\frac{C_{D2}}{C_{D0}}}$

A summary of the expressions for cruise endurance is given in Table 4.3.

Table 4.3: Maximum Endurance for Different Aircraft

Engine Type	Maximum Endurance
Turbojet	$J^* = \frac{1}{2S_{FC} \sqrt{C_{D0} C_{D2}}} \ln \left(\frac{W_c}{W_d} \right)$
Turbofan	No analytic solution
Turboprop	$J^* = \frac{1}{2S_{FC}} \left(\sqrt{\frac{2C_{D0} C_{D2}}{3\rho S}} \sqrt{\frac{C_{D2}}{3C_{D0}}} \right)^{-1} \left(\frac{1}{\sqrt{W_d}} - \frac{1}{\sqrt{W_c}} \right)$
All-Electric	$J^* = \frac{3^{3/4} (Q_c - Q_d) U \sqrt{\rho S}}{2^{5/2} W^{3/2} C_{D0}^{3/4} C_{D2}^{1/4}}$

¹Approximate analytical solution provided in Section 3.4.2

The optimal flight strategy for each aircraft can be summarized as follows:

- Turbojet and turbofan aircraft should be flown at maximum thrust in climb, idle thrust in descent, and at optimal airspeed in climb, cruise, and descent.
- Turboprop and all-electric aircraft should be flown at maximum thrust in climb, idle thrust in descent, and at optimal airspeed in climb, cruise, and descent. Furthermore, to maximize endurance, they should fly at the lowest possible cruising altitude.
- For all aircraft, the climb performance greatly impacts the cruise endurance. However, for turbojet and turbofan aircraft, it is possible to reduce the thrust profile in climb while achieving a near-optimal cruise endurance.
- The head and tailwind does not affect the optimal airspeed or thrust profiles, nor does it impact the total endurance. However, the final position and groundspeed will depend on the wind speed.

From Table 4.2, there may be discontinuities in the optimal airspeed at the switching instances t_c and t_d . The optimal airspeed profiles represent a target airspeed for the pilot to follow, and at the switching instances the aircraft would need to adjust its speed to match the target airspeed.

Similarly, the optimal thrust profile is not continuous at the switching instances either. However, the results are consistent with current airline practices. The FAA suggests using maximum thrust as a possible option for climb, and suggests using the minimum positive value of thrust in descent [65].

Chapter 5

Conclusions

In this thesis, a unified energy-depletion model was developed and used to solve the maximum endurance problem of fixed-wing aircraft. The problem was solved in cruise using an optimal control framework, and for climb, cruise, and descent using a hybrid optimal control framework. The advantage of the unified energy model is that the solution framework can be applied to both fuel-burning and all-electric aircraft. Furthermore, the use of an optimal and a hybrid optimal framework allowed the development of analytical solutions. Analytical solutions are advantageous because they provide insight into the physical properties of the problem, including sensitivities and state dependencies. The advantage of a state-feedback solution was illustrated in Chapter 2 with an example, which proved that the optimal state-feedback solution always outperforms a constant airspeed solution for a turbojet in cruise.

For each aircraft type (turbojet, turbofan, turboprop, and all-electric) a specific solution was provided. In the case of the turbofan aircraft, no exact analytical solution was provided since the problem required solving a fifth order polynomial. However, an approximate analytical solution was proposed for the turbofan in cruise using a first iteration of Newton's method. Furthermore, the turbofan solution was compared with data obtained from a rehosted Boeing 737 FMS and it was shown that the approximate analytical solution was very close to optimal.

5.1 Main Conclusions

The main results of this thesis can be summarized as follows:

- For most aircraft configurations, the use of an optimal control framework allowed analytical solutions to be derived. These were used to calculate the sensitivity of the solution to altitude, as well as to illustrate the physical dependencies of the solutions. The only aircraft configuration for which no analytical solution was possible was the turbofan.
- In order to maximize the cruise endurance, fixed-wing aircraft should be flown with maximum thrust in climb, and minimum (idle) thrust in descent.
- The results showed that the turboprop and all-electric aircraft should be flown at the lowest possible altitude to maximize endurance.

5.2 Extensions

Some possible extensions to the work provided in this thesis include

- Extending the energy-depletion model to hybrid-electric aircraft such that the energy stored in both fuel and battery charge could be optimized as a trade-off problem,
- Allowing non-level cruise or periodic cruise, which may prove to be better in certain applications,
- Including lateral flight and turn maneuvers,
- Introducing path constraints to the flight such that the aircraft remains within a given area, which would be more realistic for typical endurance mission applications,
- Explicitly include the physical constraints of the system such as the stall speed and maximum speed into the mathematical problem formulation, and
- Increasing the complexity of the models, for example:
 - using a more complex battery model for the all-electric aircraft,

- including altitude effects in the specific fuel consumption model, and
- using a more detailed model for wind.

Bibliography

- [1] I. A. T. A. (IATA), “Iata forecasts passenger demand to double over 20 years.”
- [2] *A Matter of Time: Air Traffic Delay in Europe*, vol. 2, 2007. [Online]. Available: <https://www.eurocontrol.int/sites/default/files/publication/files/tat2-air-traffic-delay-europe-2007.pdf>
- [3] T. Tomic, K. Schmid, P. Lutz, A. Domel, M. Kassecker, E. Mair, I. L. Grix, F. Ruess, M. Suppa, and D. Burschka, “Toward a fully autonomous uav: Research platform for indoor and outdoor urban search and rescue,” *IEEE robotics & automation magazine*, vol. 19, no. 3, pp. 46–56, 2012.
- [4] A. s. o. H.-Q. MIR Innovation. Inspection and maintenance solutions for power transmission systems. [Online]. Available: <http://mir-innovation.hydroquebec.com/mir-innovation/en/transmission-solutions-uav.html>
- [5] U. D. of Homeland Security, “Cbp to test the operational use of small unmanned aircraft systems in 3 u.s. border patrol sectors,” September 2017. [Online]. Available: <https://www.cbp.gov/newsroom/national-media-release/cbp-test-operational-use-small-unmanned-aircraft-systems-3-us-border>
- [6] M. Reinecke and T. Prinsloo, “The influence of drone monitoring on crop health and harvest size,” in *Next Generation Computing Applications (NextComp), 2017 1st International Conference on*. IEEE, 2017, pp. 5–10.
- [7] N. Aeronautics and S. A. (NASA), “Drones see second life mapping hurricanes – nasa’s hs3 program,” August 2017. [Online]. Available: <https://www.nasa.gov/content/drones-see-second-life-mapping-hurricanes-nasa-s-hs3-program/>

- [8] E. Airbus, “Fan the future of electric aircraft,” *Available online: company. airbus.com/responsibility/airbus-efan-the-future-of-electric-aircraft.html (accessed on 26 October 2017)*, 2017.
- [9] A. Beutel, “Nasa electric research plane gets x number, new name,” 2016.
- [10] A. E. Bryson and Y.-C. Ho, *Applied Optimal Control: Optimization, Estimation, and Control*. Taylor & Francis, 1975.
- [11] R. F. Stengel, *Optimal Control and Estimation*. Dover Publications Inc., 1994.
- [12] D. Liberzon, *Calculus of Variations and Optimal Control Theory: A Concise Introduction*. Princeton University Press, 2012.
- [13] M. Athans and P. L. Falb, *Optimal Control: an Introduction to the Theory and its Applications*. McGraw-Hill, 1966.
- [14] H. J. Sussman and J. C. Willems, “300 years of optimal control: from the brachystochrone to the maximum principle,” *IEEE Control Systems*, vol. 17, no. 3, pp. 32–44, June 1997.
- [15] A. Miele, *Mathematical Optimization Techniques*, 1963, ch. A survey of the problem of optimizing flight paths of aircraft and missiles, pp. 3–32.
- [16] ———, “The calculus of variations in applied aerodynamics and flight mechanics,” *Optimization Techniques with Applications to Aerospace Systems*, pp. 104–105, 1962.
- [17] A. Pakniyat, “Optimal Control of Deterministic and Stochastic Hybrid Systems: Theory and Applications,” Ph.D. dissertation, McGill University, Montreal, Sep. 2016.
- [18] J. A. Sorensen, S. A. Morello, and H. Erzberger, “Application of Trajectory Optimization Principles to Minimize Aircraft Operating Costs,” *18th IEEE Conference on Decision and Control including the Symposium on Adaptive Processes*, pp. 415–421, Dec. 1979.
- [19] J. W. Burrows, “Fuel-optimal aircraft trajectories with fixed arrival times,” *Journal of Guidance, Control, and Dynamics*, vol. 6, no. 1, pp. 14–19, 1983. [Online]. Available: <http://dx.doi.org/10.2514/3.19796>

- [20] S. Vilardaga and X. Prats, “Operating cost sensitivity to required time of arrival commands to ensure separation in optimal aircraft 4d trajectories,” *Transportation Research Part C: Emerging Technologies*, vol. 61, pp. 75–86, Dec. 2015. [Online]. Available: <http://www.sciencedirect.com/science/article/pii/S0968090X15003630>
- [21] J. Villarroel and L. Rodrigues, “Optimal control framework for cruise economy mode of flight management systems,” *Journal of Guidance, Control, and Dynamics*, pp. 1022–1033, 2016.
- [22] A. Botros, “Minimizing direct operating cost for turbojet and turboprop aircraft in cruise,” Master’s thesis, Concordia University, Montreal, Quebec, Canada, August 2017.
- [23] J. García-Heras, M. Soler, and F. J. Sáez, “A Comparison of Optimal Control Methods for Minimum Fuel Cruise at Constant Altitude and Course with Fixed Arrival Time,” *Procedia Engineering*, vol. 80, pp. 231–244, Jan. 2014. [Online]. Available: <http://www.sciencedirect.com/science/article/pii/S187770581401176X>
- [24] N. Kim, S. Cha, and H. Peng, “Optimal control of hybrid electric vehicles based on pontryagin’s minimum principle,” *IEEE Transactions on Control Systems Technology*, vol. 19, no. 5, pp. 1279–1287, 2011.
- [25] C. W. Bert, “Range and endurance of turboprop, turbofan, or piston-propeller aircraft having wings with or without camber,” *Aircraft Design*, vol. 2, no. 4, pp. 183–190, December 1999.
- [26] D. P. Raymer, “Approximate method of deriving loiter time from range,” *Journal of Aircraft*, vol. 41, no. 4, pp. 938–940, July-August 2004.
- [27] J. Villarroel, “An Optimal Control Framework for Flight management Systems,” Master’s thesis, Concordia University, Montreal, Feb. 2015.
- [28] M. Kaptsov, “An energy efficient optimal control framework for general purpose flight management systems,” Master’s thesis, Concordia University, 2017.
- [29] M. Kaptsov and L. Rodrigues, “Electric aircraft flight management systems: Economy mode and maximum endurance,” *Journal of Guidance, Control, and Dynamics*, vol. 41, no. 1, pp. 285–290, January 2018.

- [30] C. W. Bert, "Prediction of range and endurance of jet aircraft at constant altitude," *Journal of Aircraft*, vol. 18, no. 10, pp. 890–892, Oct. 1981. [Online]. Available: <https://0-arc.aiaa.org/mercury.concordia.ca/doi/10.2514/3.44738>
- [31] A. Pakniyat and P. E. Caines, "Hybrid optimal control of an electric vehicle with a dual-planetary transmission," *Nonlinear Analysis: Hybrid Systems*, vol. 25, pp. 263–282, 2017.
- [32] I. M. Ross and C. N. D'Souza, "Hybrid optimal control framework for mission planning," *Journal of Guidance, Control, and Dynamics*, vol. 28, no. 4, pp. 686–697, 2005.
- [33] M. Soler, A. Olivares, and E. Staffetti, "Hybrid optimal control approach to commercial aircraft trajectory planning," *Journal of Guidance, Control, and Dynamics*, vol. 33, no. 3, pp. 985–991, 2010.
- [34] A. Franco and D. Rivas, "Optimization of multiphase aircraft trajectories using hybrid optimal control," *Journal of Guidance, Control, and Dynamics*, vol. 38, no. 3, pp. 452–467, 2015.
- [35] M. Soler, A. Olivares, E. Staffetti, and D. Zapata, "Framework for Aircraft Trajectory Planning Toward an Efficient Air Traffic Management," *Journal of Aircraft*, vol. 49, no. 1, pp. 341–348, Jan. 2012. [Online]. Available: <https://0-arc.aiaa.org/mercury.concordia.ca/doi/10.2514/1.C031490>
- [36] G. Sachs and T. Christodoulou, "Endurance increase by cyclic control," *Journal of Guidance*, vol. 9, no. 1, pp. 58–63, January-February 1986.
- [37] P. K. Menon, G. D. Sweriduk, and A. H. Bowers, "Study of near-optimal endurance-maximizing periodic cruise trajectories," *Journal of Aircraft*, vol. 44, no. 2, pp. 393–398, March-April 2007.
- [38] J. Villarroel and L. Rodrigues, "An optimal control framework for the climb and descent economy modes of flight management systems," *IEEE Transactions on Aerospace and Electronic Systems*, vol. 52, no. 3, pp. 1227–1240, Jun. 2016.
- [39] Y. Zhao and P. Tsiotras, "Analysis of Energy-Optimal Aircraft Landing Operation

- Trajectories,” *Journal of Guidance, Control, and Dynamics*, vol. 36, no. 3, pp. 833–845, 2013. [Online]. Available: <http://dx.doi.org/10.2514/1.57779>
- [40] L. Stell, “Prediction of top of descent location for idle-thrust descents,” in *9th USA/Europe Air Traffic Management R&D Seminar, Berlin, Germany*, 2011.
- [41] L. Rodrigues, “A unified optimal control approach for maximum endurance and maximum range,” *IEEE Transactions on Aerospace and Electronic Systems*, vol. 54, no. 1, pp. 385–391, February 2018.
- [42] H. Erzberger and H. Lee, “Constrained optimum trajectories with specified range,” *Journal of Guidance and Control*, vol. 3, no. 1, pp. 78–85, February 1980.
- [43] R. S. F. Patron, R. M. Botez, and D. Labour, “Flight trajectory optimization through genetic algorithms coupling vertical and lateral profiles,” in *The ASME 2014 International Mechanical Engineering Congress and Exposition*, November 2014.
- [44] A. Franco and D. Rivas, “Minimum-cost cruise at constant altitude of commercial aircraft including wind effects,” *Journal of Guidance, Control, and Dynamics*, vol. 34, no. 4, pp. 1253–1260, 2011.
- [45] W. E. Randle, C. A. Hall, and M. Vera-Morales, “Improved Range Equation Based on Aircraft Flight Data,” *Journal of Aircraft*, vol. 48, no. 4, pp. 1291–1298, Jul. 2011. [Online]. Available: <https://0-arc.aiaa.org/mercury.concordia.ca/doi/10.2514/1.C031262>
- [46] A. CHAKRAVARTY, “Four-dimensional fuel-optimal guidance in the presence of winds,” *Journal of Guidance, Control, and Dynamics*, vol. 8, no. 1, pp. 16–22, 1985. [Online]. Available: <http://dx.doi.org/10.2514/3.19929>
- [47] F. J. Hale and A. R. Steiger, “Effects of Wind on Aircraft Cruise Performance,” *Journal of Aircraft*, vol. 16, no. 6, pp. 382–387, Jun. 1979. [Online]. Available: <https://0-arc.aiaa.org/mercury.concordia.ca/doi/10.2514/3.58535>
- [48] *U.S. Standard Atmosphere*. Washington, D.C.: NASA, October 1976.

- [49] J. D. Anderson, *Aircraft Performance and Design*. McGraw-Hill Inc., 1999.
- [50] A. F. El-Sayed, *Fundamentals of Aircraft and Rocket Propulsion*. Springer, 2016.
- [51] J. D. Mattingly, *Elements of propulsion: gas turbines and rockets*. American Institute of Aeronautics and Astronautics, 2006.
- [52] J. L. Speyer and D. H. Jacobson, “Necessary and sufficient conditions for optimally for singular control problems; a transformation approach,” *Journal of Mathematical Analysis and Applications*, vol. 33, no. 1, pp. 163–187, Jan. 1971. [Online]. Available: <http://www.sciencedirect.com/science/article/pii/0022247X71901909>
- [53] N. Nguyen, “Singular Arc Time-Optimal Climb Trajectory of Aircraft in a Two-Dimensional Wind Field,” in *AIAA Guidance, Navigation, and Control Conference and Exhibit*. American Institute of Aeronautics and Astronautics, Aug. 2006. [Online]. Available: <http://arc.aiaa.org/doi/abs/10.2514/6.2006-6598>
- [54] H. J. Kelley, “A second variation test for singular extremals,” *AIAA Journal*, vol. 2, no. 8, pp. 1380–1382, Aug. 1964. [Online]. Available: <http://arc.aiaa.org/doi/10.2514/3.2562>
- [55] C. Johnson and J. Gibson, “Singular solutions in problems of optimal control,” *IEEE Transactions on Automatic Control*, vol. 8, no. 1, pp. 4–15, Jan. 1963.
- [56] G. J. Miel, “Majorizing sequences and error bounds for iterative methods,” *Mathematics of Computation*, vol. 34, no. 149, pp. 185–202, January 1980.
- [57] A. Galantai, “The theory of newton’s method,” *Journal of Computational and Applied Mathematics*, vol. 124, pp. 25–44, January 2000.
- [58] T. Yamamoto, “Historical developments in convergence analysis for newton’s and newton-like methods,” *Journal of Computational and Applied Mathematics*, vol. 124, pp. 1–23, December 2000.
- [59] M. Longmuir and N. A. Ahmend, “Commercial aircraft exterior cleaning optimization,” *Journal of Aircraft*, vol. 46, no. 1, pp. 284–290, February 2009.

- [60] “King air 350i.” [Online]. Available: <http://beechcraft.txtav.com/en/king-air-350i>
- [61] E. Joubert, D. Chapuis, D. Esteyne, J.-C. Lambert, O. Siri, and D. Müller-Wiesner, “The e-fan all electrical aircraft demonstrator and its industrialization,” in *Proceedings of the 30th Congress of the International Council of the Aeronautical Sciences*, 2016.
- [62] MathWorks. Solve equations numerically. [Online]. Available: <https://www.mathworks.com/help/symbolic/solve-equations-numerically.html>
- [63] B737 technical specifications. [Online]. Available: <http://www.b737.org.uk/techspecs/detailed.htm>
- [64] R. A. Society. Bright sparks - the quest for electric speed. [Online]. Available: <https://www.aerosociety.com/news/bright-sparks-the-quest-for-electric-speed/>
- [65] *Pilot’s Handbook of Aeronautical Knowledge (FAA-H-8083-25B)*. FAA, 2016, ch. Aircraft Performance.